Nonlinear Dyn (2021) 103:343–366
https://doi.org/10.1007/s11071-020-06120-5

ORIGINAL PAPER

On nonlinear energy flows in nonlinearly coupled oscillators with equal mass

Chengen Wang · Keegan J. Moore

Received: 14 May 2020 / Accepted: 28 November 2020 / Published online: 5 January 2021

Abstract Due to the near monopoly held by nonlinear energy sinks in the study of targeted energy transfer, little research has been done on the flow of mechanical energy between oscillators with comparable mass. The goal of the present paper is to investigate the flow of mechanical energy between two nonlinearly coupled oscillators with comparable mass that arise due to the breaking of dynamic reciprocity. The first oscillator represents the prototypical linear oscillator (LO), whereas the second oscillator represents a nonlinear oscillator (NO) that is nonlinearly coupled to the LO only. By breaking dynamic reciprocity, one-way energy propagation is achieved in the system, such that energy can only be irreversibly transferred from the NO to the LO. As such, the NO is isolated from the LO for physically reasonable energies whenever it is not directly excited. Moreover, when the NO is directly excited, there exist regimes where the LO, despite being linear and of comparable mass to the NO, behaves like a nonlinear energy sink and parasitically and irreversibly absorbs energy from the NO. The theoretical portion of this works employs direct numerical simulation of the structure to explore the strongly nonreciprocal dynamics and resulting energy transfers. The theoretical results are then verified through experimental measurements of a comparable structure. The present study promotes a new paradigm for investigating energy transfer in mechanical structures and opens the way for passively controlling the flow of energy in complex mechanical systems.

Keywords Energy transfer · Vibration isolation · Nonlinear normal modes · Nonlinear dynamics · Nonreciprocity · Nonlinear energy sink

C. Wang · K. J. Moore (✉)
Department of Mechanical and Materials Engineering, University of Nebraska-Lincoln, Lincoln, NE 68588, USA
e-mail: kmoore@unl.edu

1 Introduction

Recent research on energy transfer in mechanical systems has been dominated by the phenomena of targeted energy transfer, which is a form of passive, directional energy transfer [1, 2]. More specifically, targeted energy transfer is traditionally defined as an irreversible transfer of mechanical energy from a primary structure to a set of local attachments called nonlinear energy sinks (NESs). A NES typically possesses a linear viscous damper, low mass relative to the primary structure, and an essential nonlinearity, i.e., a strong nonlinearity (of order 1) and no linear stiffness. Although the NES is typically studied theoretically without any linear stiffness, zero linear stiffness often cannot be achieved in experimental implementations and, in this case, any linear stiffness

must be weak enough that the frequency associated with the NES at low excitation levels is less than that of the modes of the primary structure. Since its inception, the phenomena of targeted energy transfer and the study of NESs have blossomed into a rich field of research with many applications [3–13] and many different types including those with polynomial nonlinearities [14–17], bi-stable elements [18–20], and vibro-impacts [21–24].

More recent research has implemented NESs into hierarchical lattices as a means to break dynamic reciprocity and achieve uni-directional propagation of energy [25–27]. In these studies, a lattice structure was constructed using a combination of large scales (oscillators with large mass) and small scales (NESs). Specifically, each unit cell in the lattice possessed a single large scale that was linearly coupled to the ground and nonlinearly coupled to the small scale. Individual unit cells were connected to each other by coupling the small scale in the left cell to the large scale in the right cell. Thus, all small scales were coupled to two larges scales except for the rightmost scale, which was only nonlinearly coupled to the large scale in its unit cell. For this lattice, it was found that when the leftmost unit cell was excited, energy was able to freely propagate across the lattice where it was reflected back. However, when the rightmost unit cell was excited, the energy became trapped in that unit cell and was unable to propagate across the lattice. The emergence of uni-directional energy propagation in this lattice arose because the energy became localized in the small scale due to irreversible energy transfers. Further studies have revealed that the presence of a NES in the system is not necessary to break dynamic reciprocity and create preferential directions of energy transfer [28–32].

Despite these recent developments in realizing uni-direction propagation of energy through the breaking of dynamic reciprocity, research into energy transfer mechanisms is still dominated by the phenomena of targeted energy transfer through the use of NESs. Consequently, few studies have been done on the mechanisms that govern energy transfers in systems with components with comparable mass. For example, the studies performed in [33, 34] investigated energy transfers between two oscillators, a linear oscillator (LO) and a nonlinear oscillator (NO), with equal mass and both weak and strong nonlinearities. In both studies, weak nonlinearity was used to couple the two oscillators together and in [33] a strong grounding nonlinearity was included in the NO. The authors found that energy could be transferred from both the LO to the NO and the NO to the LO. However, the authors proved that these energy exchanges could only occur during internal resonances (IRs) and, outside of IRs, no energy could be exchanged between the two oscillators. However, as demonstrated in the phenomena of targeted energy transfer, the presence of strong coupling nonlinearity often results in nonlinear energy exchanges and transfers both during and away from IRs. Thus, further research into the mechanisms of energy transfer between components of equal mass is necessary.

Multiple analytical and experimental methods have been developed to study the flow of mechanical energy throughout the structure. In [14], the authors used the method of nonsmooth temporal transformations [35] to study the transfer of energy that arises due to a 1:1 subharmonic resonance between two oscillators. Vakakis and Gendelman [15] investigated energy transfers in two oscillators with weak linear coupling where one oscillator had strong linear grounding stiffness and the other had strong nonlinear grounding stiffness. They transformed the equations of motion using action-angle variables and studied the energy transfer that arises on a 1:1 resonance manifold. Second, they employed the method of complexification averaging [36] under the assumption of 1:1 resonance and computed approximate solutions to the strongly nonlinear equations of motion. Using the results from both methods, they showed that the 1:1 resonance leads to energy pumping from the linear oscillator into the nonlinear oscillator. The method of complexification averaging has been used in many studies of energy transfer under internal resonances including [37–43]. In [33], the authors employed the method of regular perturbations to analytically study the nonlinear energy transfers between oscillators, but as mentioned before they found that transfers only arose during internal resonances and resonance captures. The method of multiple scales [44] has also been used to study energy transfers such as in [45, 46] and, combined with the method of harmonic balance, in [47].

Several approaches have been implemented to study nonlinear energy transfers directly from experimental measurements. In [48], the authors derived a method to compute the instantaneous energy in each

degree of freedom by picking successive peaks in the kinetic energy and fitting a shape preserving spline from these points. One issue with this approach is that if any degrees of freedom exchange energy at any time, then a beating pattern will appear in the kinetic energy that will not be captured by the method proposed in [48]. Moreover, the sum of the estimated total energies in each degree of freedom will be larger than the actual total energy in the system. In [25, 26], the authors identified representative mathematical models for each oscillator studied in the experimental system and then estimated the instantaneous energy in each mass using both the kinetic and potential energies. Any potential energy that arose from coupling springs was shared evenly between the connected oscillators without regard for how much each oscillator contributed to that potential energy. The issue with this approach is that one oscillator might have a large displacement, whereas the other might have a small displacement resulting in large relative displacement. However, it is unclear which oscillator is contributing the most to the resulting potential energy and whether dividing the energy equally is physically accurate. Another approach to studying energy transfers that is commonly used when an NES is installed on a primary linear system is to assign all of the potential energy that arises from the coupling to the NES [49–52]. The instantaneous energy in the NES is then defined as the sum of the kinetic energy of the NES and all potential energies that involve the displacement of the NES. This approach incurs the same issue as the previous in that some of the energy contributed by the primary system is included in the energy of the NES. Recently, Silva et al. [52] investigated the flow of energy from a primary linear system into an NES using power flow calculated using the derivative of the kinetic, potential, and dissipated energies. Using the power flow, the authors found that low damping results in a backflow of energy from the NES into the primary structure, such that the two masses exchange energy instead of irreversibly transferring it. With large enough damping, the authors found that no backflow from the NES occurs, such that the energy is irreversibly transferred from the primary system into the NES.

The purpose of the present paper is to investigate the flow of energy between two oscillators of equal mass. The first oscillator represents the prototypical LO, whereas the second represents a NO that is nonlinearly coupled to the LO only. Throughout this research, we explore how energy flows and is shared between these two oscillators by analyzing the instantaneous energy in each oscillator, which is estimated from the kinetic energies. The advantage of this approach is that it can be applied directly to experimental measurements provided the mass of each oscillator is known and, more importantly, it avoids mixing the contributions of each oscillator in the potential energies. We also use nonlinear normal modes (NNMs) [53, 54] to explain the various transfers of energies observed. We adopt the definition that NNMs are time-periodic oscillations that may be regarded as nonlinear extensions of linear normal modes. They are synchronous in the absence of internal resonances (IR); however, when IRs arise, the NNMs interact with each other through strongly nonlinear energy exchanges and the resulting oscillations are nonsynchronous with multiple NNMs participating.

To enhance clarity, we provide a summary of the novel findings of this research here. First, we demonstrate that irreversible targeted energy transfer (TET) can be achieved in the opposite direction that is normally observed in TET studies. Specifically, we show that, when the NO is excited in this system, the LO can behave like a parasite and irreversibly steal energy from the NO. Such behavior is the opposite of the traditional TET that is observed in LO–NES systems where energy is irreversibly transferred from the LO to the NES. Second, studies of nonlinear energy transfer and IRs typically focus on low-to-high frequency transfers of energy; however, we show that both low-to-high and high-to-low frequency energy transfers arise due to a 3:1 IRs in the system. We also show that the high-to-low transfers always result in an exchange of energy between the two masses, whereas the low-to-high transfers can result in either an exchange of energy or an irreversible transfer of energy from the NO to the LO. Third, we demonstrate that there is a preferential direction of energy flow, from the NO to the LO, below a certain excitation threshold. This preference is result from nonlinear localization where the energy prefers to remain isolated in the LO when it is excited below that threshold instead of transferring into the NO. The NO exhibits similar localization if it is excited, but the threshold for this behavior is much lower than for the LO, which gives rise to the preferential direction of

energy transfer. The rest of this paper is divided as follows: Sect. 2 presents a theoretical study of the LO–NO system along with an explanation of how the instantaneous energy in each oscillator is computed; Sect. 3 presents the design of the experimental systems, the system identification procedure employed, and the resulting mathematical model, and an experimental verification of the theoretical results; and, finally, Sect. 4 provides some concluding remarks.

2 Theoretical investigation of targeted vibration isolation

2.1 Theoretical system

In this research, we investigate the strongly nonlinear energy transfers that arise in a system composed of two oscillators with comparable mass as depicted in Fig. 1. The first oscillator is linearly coupled to the ground and represents the typical linear oscillator (LO) in the system, whereas the second oscillator is nonlinearly coupled to the LO and is termed the nonlinear oscillator (NO). Note that, in typical TET studies, the LO is considered to be the primary system and NO is considered to be a strongly nonlinear attachment that is installed on the LO to mitigate unwanted vibrations. However, we caution the reader that this is not our objective in this research and this viewpoint should not be adopted. Rather, our objective is to passively control the flow of energy between the two masses, such that energy is allowed to transfer from the NO to the LO, but not from the LO to the NO. The nondimensional equation of motion governing the LO is

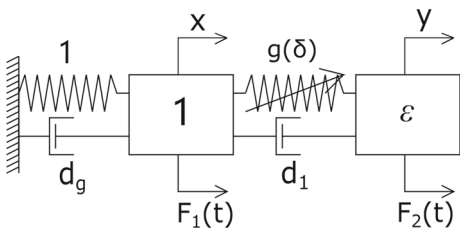

Fig. 1 The theoretical schematic of the system, with $g(\delta) = a(x-y)^3 + k(x-y)$

$$\ddot{x} + d_1\dot{x} + k_1 x + d_2(\dot{x} - \dot{y}) + k_2(x-y) + \alpha(x-y)^3 = F_1(t), \tag{1}$$

and the nondimensional equation of motion governing the NO is

$$\varepsilon\ddot{y} + d_2(\dot{y} - \dot{x}) + k_2(y-x) + \alpha(y-x)^3 = F_2(t), \tag{2}$$

where $x(t)$ and $y(t)$ are the displacements of the LO and NO, respectively.

In typical studies of targeted energy transfer, the mass of the NO is chosen to be relatively small compared to the mass of the LO, usually $\varepsilon < 0.1$), which enables energy to irreversibly transfer from the LO to the NO. In this research, we consider the case where the mass of the NO is comparable to that of the LO and will show that this results in an energy-transfer scheme that is the exact opposite of what is observed when the mass of the NO is small. Specifically, we consider the case where the mass of the NO is $\varepsilon = 1$, such that the two parameters have equal masses. The values of the rest of the parameters are chosen as follows: $k_1 = 1$, $d_1 = 0.01$, $d_2 = 0.001$, $k_2 = 0$, $\alpha = 1$. Additionally, we consider two impulsive loading scenarios: first, only the LO is impulsively excited for zero initial conditions such that $F_1(t) = v_0\delta(t)$ and $F_2(t) = 0$ (loading scenario I); second, only the NO is impulsively excited for zero initial conditions such that $F_1(t) = 0$ and $F_2(t) = v_0\delta(t)$. The implementation of the impulsive forcing is discussed in the next subsection.

To help facilitate the discussion of the behavior of this system, we compute the nonlinear normal modes (NNMs) of the corresponding Hamiltonian system (i.e., without damping or external forces) using numerical continuation [54, 55]. We adopt the definition that NNMs are time-periodic oscillations that may be regarded as nonlinear extensions of linear normal modes. They are synchronous in the absence of internal resonances (IR); however, when IRs arise, the NNMs interact with each other through strongly nonlinear energy exchanges and the resulting oscillations are nonsynchronous with multiple NNMs participating. The resulting NNMs are presented in Fig. 2 along with two subharmonic branches shown as the dashed and dash-dotted lines. The first and second NNMs are labeled using the notation $S11+$ and $S11-$, respectively, where the letter S represents a symmetric

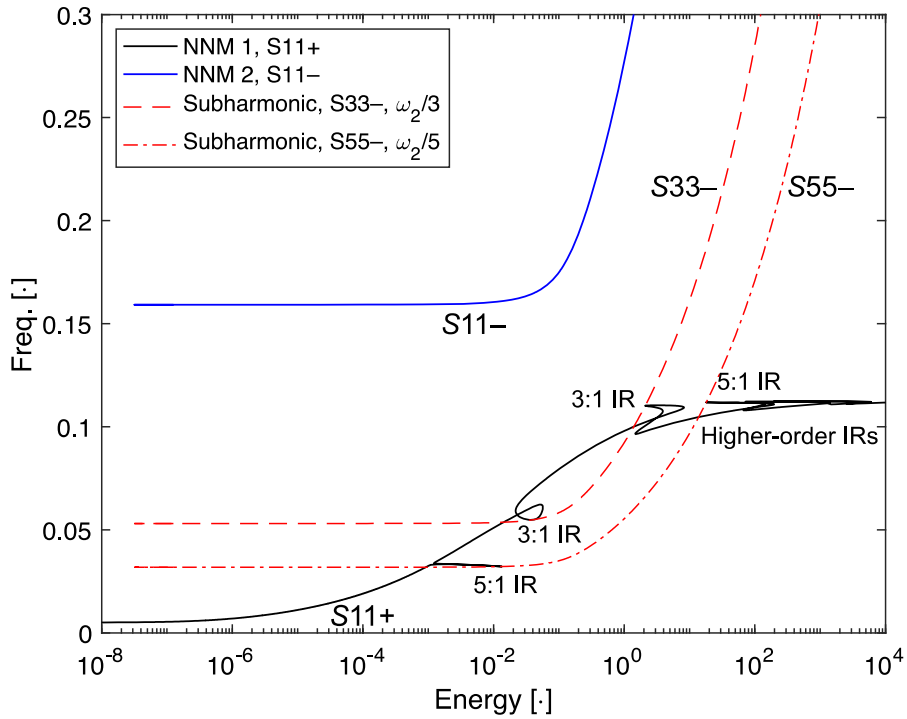

Fig. 2 The two NNMs for the corresponding Hamiltonian system. The dashed and dash-dotted line are created by dividing the frequency of the second NNM by 3 and 5, respectively, and show which tongues correspond to 3:1 and 5:1 IRs

NNM, the indices represent that each mass oscillates with the same dominant frequency, and the + (–) represents in-phase (out-of-phase) motion. The subharmonic branches are labeled as *S*33– and *S*55–, and they are obtained by dividing the frequency of the second NNM by 3 and 5, respectively. Note that the first NNM can be partitioned into two linear limiting regions at low and high energies and a single nonlinear transition region that connects the two linear portions. In contrast, the second NNM can only be divided into two separate regimes: first a linear limiting regime at low energy and a nonlinear region where the frequency increases to infinity. We note further that although a 5:1 IR is the first tongue to emerge, the addition of damping in the system prevents this IR from materializing. However, the damping does not prevent the first 3:1 IR from occurring in the dynamics and we will investigate the effect of this 3:1 IR in the following sections.

2.2 Estimation of instantaneous energy in each mass

Due to the strong dependence of energy a nonlinear system has, it is crucial for us to investigate the behavior of the system under different energy levels. To this end, we implement the impulsive forcing described in the previous subsection as an initial velocity, such that the loading scenarios (LSs) are converted to the following initial conditions: LS I—$x(0) = y(0) = \dot{y}(0) = 0, \dot{x}(0) = v_0$; and LS II—$x(0) = \dot{x}(0) = y(0) = 0, \dot{y}(0) = v_0$. To explore the energy-dependent dynamics of the system, we simulated its response for each LS for 2000 linearly spaced values of v_0 from 0.001 to 1. Rather than analyzing the behavior of the system for each initial velocity individually, we are interested in investigating changes in the overall behavior of the system, especially the flow of energy between the two masses. Thus, for each simulation, we calculate the instantaneous total energy in the system and estimate the instantaneous total energy in each mass.

The instantaneous total energy in each mass is computed using a similar approach to that described by Sapsis et al. [48], which consists of fitting a spline curve to the peaks of the kinetic energies to obtain the instantaneous total energy in each mass. Instead of fitting splines to the peaks of the kinetic energies, we estimate the instantaneous energy in each mass by first estimating the instantaneous amplitude of the kinetic energies using the *imdilate* function in MATLAB® and low-pass filter the result. The *imdilate* function is

actually intended for image dilation, which is an operator in mathematical morphology that grows regions around white pixels and shrinks regions around black pixels. In our implementation, the *imdilate* function produces a nonsmooth estimate of the instantaneous amplitude of the kinetic energy and the low-pass filter is applied to smooth the estimate. The low-pass filter is implemented using a third-order Butterworth filter with a cutoff frequency of 0.1. An example of the estimated total energies in each mass is presented in Fig. 3 for LS I and an initial velocity of $v_0 = 0.5$. A major benefit of this approach is that it captures any exchanges of energy that occur between the two masses, which appear as slow modulations of the amplitude of the kinetic energies and slow oscillations in the estimated energies. In fact, the slow oscillations in the estimated energies observed after a time of 100 in Fig. 3 indicate a strongly nonlinear exchange of energy where energy is transferred from the LO to the NO. A second benefit of this approach is that it avoids having to partition and shares the potential energy between the two masses as was done in previous research such as in [25, 26].

2.3 Loading scenario I: LO excited

As stated previously, our overall objective is to study how the flow of energy between the two masses evolves as the excitation amplitude increases. To achieve this objective, we estimate the instantaneous total energy in each mass for each initial velocity and LS. Next, we normalize the instantaneous energies by dividing by the corresponding initial energy $\left(\frac{1}{2}v_0^2\right)$ and multiply by 100% to obtain the instantaneous percent energy in each mass. The instantaneous percent energies are preferable over the instantaneous total energies because they are on the same scale (0 to 100%) and provide a fair comparison across all initial velocities. By placing the energies on the same scale for all initial velocities, the instantaneous percent energies provide the means to study the evolution of the energy flows and the behavior of the system without bias toward simulations with higher initial energy. To this end, we depict the instantaneous percent energies in each mass as functions of the initial energy and time in Figs. 3 and 5 for LSs I and II, respectively. We will use the remainder of this subsection to discuss the results for LS I, and we discuss the results for LS II in the next subsection.

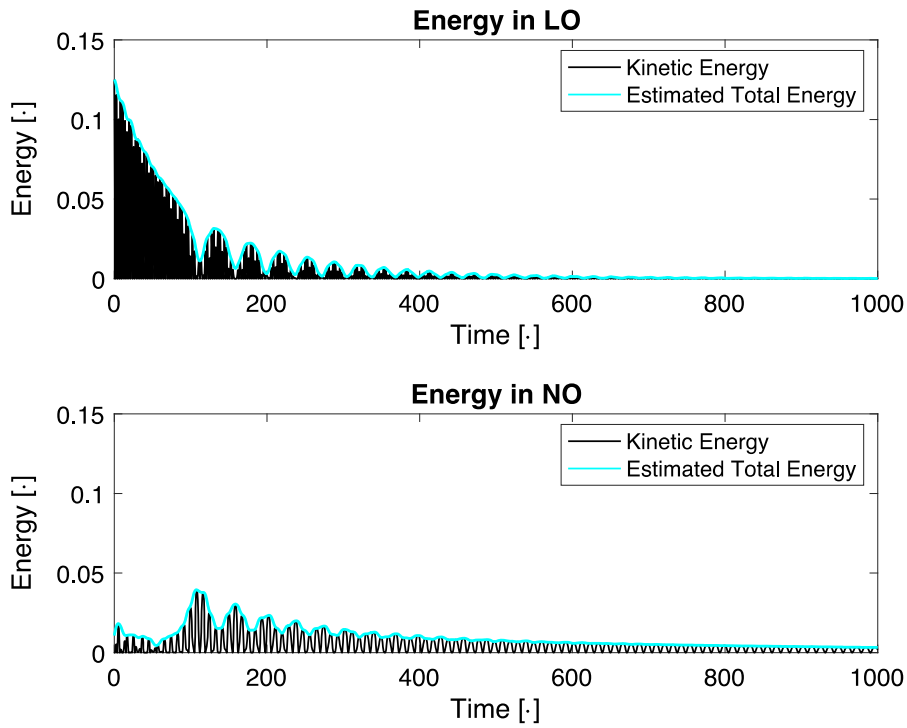

Fig. 3 Example of the estimated instantaneous total energy in each mass for LS I and $v_0 = 0.5$

Considering LS I, we find that the energy distribution can be partitioned into two separate regimes of behavior. Specifically, Regime I encloses the behavior for initial velocities below 0.32 and Regime II corresponds the behavior for initial velocities above 0.32. We find that, in Regime I, the energy isolates almost entirely in the LO for the entire duration of the response. The fact that no energy flows from the LO to the NO in this regime implies that the NO is strongly isolated from the LO and barely participates in the response. To verify that NO is isolated from the LO in this regime, we present a comparison of the displacement responses of the LO and NO for $v_0 = 0.15$ in Fig. 5a. The comparison of the displacement responses shows that the NO moves significantly slower than the LO (at a much lower frequency) and with a significantly lower amplitude. In fact, the maximum displacement of the LO is 0.148, whereas the maximum displacement of the NO is only 0.027, such that the NO displaces only 18.2% as much as the LO. In addition to the displacement time series, we also include the corresponding wavelet transform (WT) spectra [56] and comparisons of the instantaneous energy in each mass and the total grounding and coupling forces. The WT spectra depict the temporal evolution of the nonlinear normal modes (NNM) [52, 53] governing the dynamics and are shaded such that darker shading indicates higher energy content and the light-blue background indicates zero energy content. Note that the WT spectra are normalized to be on the same scales for both the LO and NO for this simulation, such that the WT spectrum of the LO can be compared with the NO for this initial velocity, but the spectra should not be compared for different initial velocities. The WT spectra reveal that the response of the LO is governed by a single component with a frequency of 1, which represents the second NNM of this system. In contrast, the response of the NO is governed by two components: the second NNM at a frequency of 1, which quickly exits the response, and the first NNM with an extremely low frequency that decreases with time to zero frequency (not shown here). Moreover, the lack of variation is in the frequency. It turns out that, in the absence of resonances, the first and second NNMs represent local modes that govern the response of the NO and LO, respectively, which explains why the NNMs are isolated to their respective masses in this response.

Without any IRs to give rise to strongly nonlinear energy exchanges between the LO and the NO, the energy should remain isolated in the LO for the duration of the response. This prediction is confirmed by the comparison of the instantaneous energies in the LO and NO, where, indeed, we find that the energy is isolated in the LO for the entire response. In fact, the LO and NO have maximum energy values of 0.0113 and 8.9×10^{-6}, respectively, such that the NO possesses at most only 0.079% of the maximum total energy. As a final validation of the isolation of the NO from the LO, we compare the total grounding force, which acts only on the LO, with the total coupling force, which is the only for acting on the NO. Moreover, the coupling force captures the force transfer (or in some sense the transmissibility) from the LO to the NO. As can be seen in the bottom of Fig. 5a, the coupling force is significantly smaller than the grounding force, such that very little of the applied force is transferred to the NO. The maximum amplitudes of the grounding and coupling forces are 0.148 and 0.0039, respectively, such that only 2.6% of the input force magnitude (0.15) is transferred to the NO.

Considering Fig. 4 again, but now for Regime II and initial velocities above 0.32, we find that the energy is no longer strictly isolated in the LO, but also flows from the LO into the NO for certain bands of initial velocities. To study these energy transfers, we consider the response of the system for an initial velocity of 0.34 (applied to the LO) and present a comparison of the displacement response of the LO and NO in Fig. 5b. Note that this initial velocity corresponds to the center of the first energy-transfer band in Fig. 4 and should also correspond to the largest amount of energy transfer in that band. The displacement response reveals that, initially, the motion of the NO is small and slow compared to that of the LO; however, after a time of approximately 50, the NO suddenly grows in amplitude followed by the appearance of a beating pattern in responses of both the NO and LO. Note that a similar beating pattern is also observed in the energy exchanges depicted in Fig. 4. Since the linear frequencies of the two NNMs are not close together, the appearance of beating in the displacement response indicates that the LO and NO are engaged in an IR which leads to the exchange of energy between the masses.

To study the IR in the dynamics, we turn to the WT spectra of the LO and NO in Fig. 5b, which reveal that

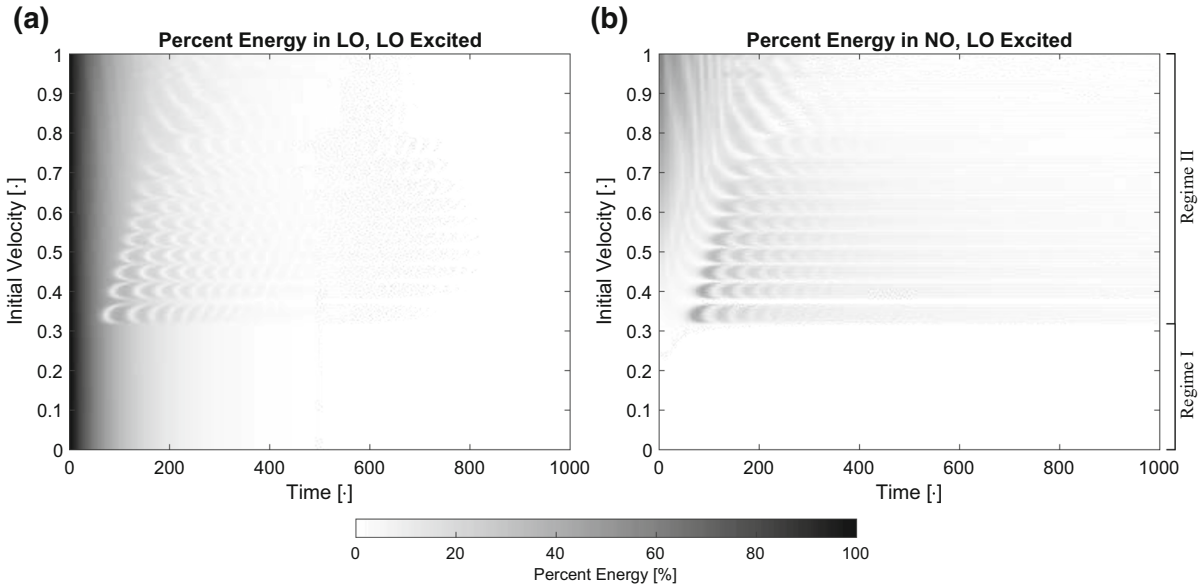

Fig. 4 The percent distribution of energy in the **a** LO and **b** NO as functions of time for LS I

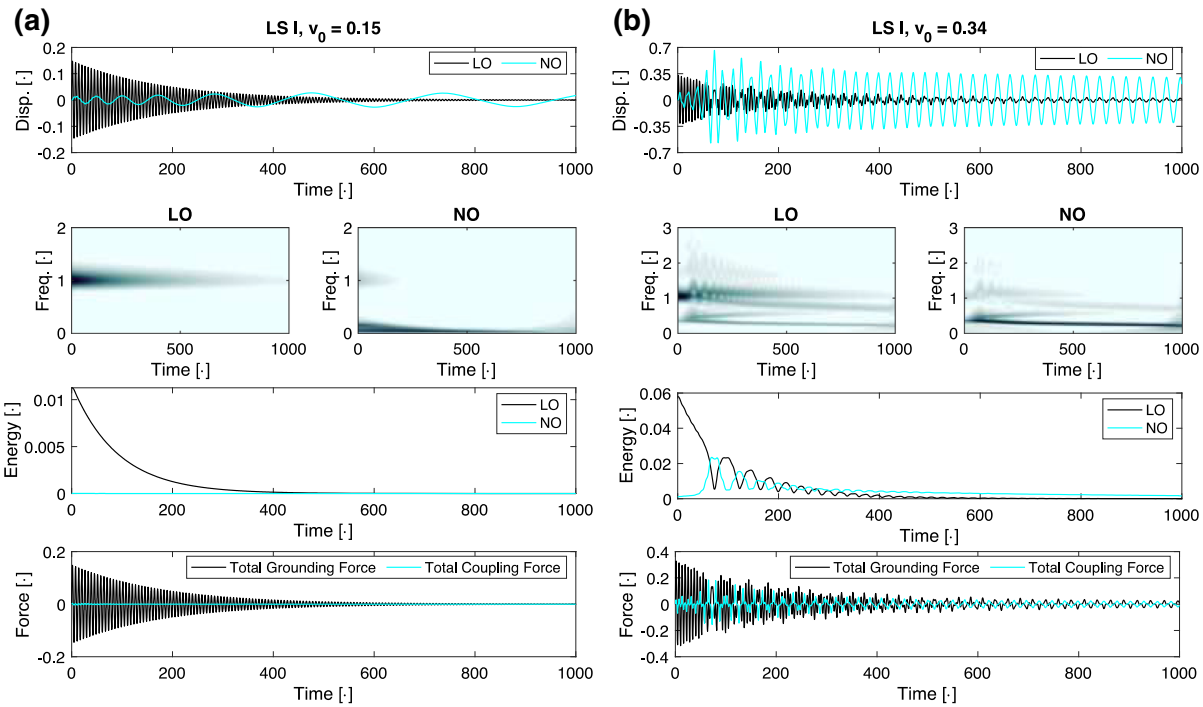

Fig. 5 Comparison of the displacement response, corresponding WT spectra, instantaneous energies for the LO and NO, and the grounding and coupling forces for LS I and initial velocities of **a** 0.15 and **b** 0.34

the responses of both the LO and NO are governed by multiple frequencies. The first and second NNMs correspond to the components with the lowest frequency and a frequency of approximately 1, whereas the other components found in the WT spectra are actually harmonics of the first NNM. As

stated previously, the darker the shading in the WT spectra, the higher the energy content at a particular time and frequency. Since the WT are normalized to the same scale, comparing them provides the means to assess where the energy is concentrated at a given time. The WT spectra reveal that, up until a time of 50, the majority of the energy is concentrated in the LO and in the second NNM; however, after a time of 50, the energy suddenly concentrates in the NO and in the first NNM. Moreover, right after a time of 50, a beating pattern appears in the WT spectrum of the LO, which further confirms the presence of an IR in the dynamics. Around a time of 50, the frequencies of the first and second NNMs are approximately 0.35 and 1.05, respectively, such that the frequency of the first NNM is one-third of that of the LO. The IR in the dynamics must, therefore, be a 3:1 IR between the first and second NNMs. Typically, IRs result in the scattering or transfer of energy from low to high frequencies in the response [1, 2, 53], but, in this case, energy is actually transferred down from a high-frequency mode (the second NNM) to a low-frequency mode (the first NNM).

The hypothesis that a 3:1 IR arises in the dynamics and gives rise to significant energy transfer from the LO to the NO is further supported by the comparison of the instantaneous total energy in each mass and the comparison of the total grounding and coupling forces. Specifically, from the comparison of the energies, we find that the majority of the energy is concentrated in LO with almost no energy stored in the NO up until a time of 50. After a time of 50, a rapid transfer of energy from the LO to the NO occurs followed by an extreme oscillating exchange of energy that corresponds with the beating pattern observed in the time series and WT spectra. A comparable pattern emerges in the comparison of the forces where, up until a time of 50, the grounding force is large in amplitude, whereas the coupling force is low in amplitude. However, after a time of 50, the coupling force grows in amplitude and a beating pattern emerges where the grounding and coupling forces have large amplitudes when the energy is concentrated in the LO and NO, respectively.

Finally, to verify that a 3:1 IR arises in the dynamics, we depict the WT spectra of both the LO and NO displacement responses as functions of total mechanical energy for initial velocities of 0.15 and 0.34 in Fig. 6a, b, respectively. On top of the WT spectra, we superimpose the NNMs of the underlying Hamiltonian system shown in Fig. 2. For an initial velocity of 0.15, shown in Fig. 6a, we find that the NO does not participate strongly in the response and that none of the IRs are activated. Although the response is close to the 5:1 IR tongue, the damping in the system most likely prevents this IR from materializing and affecting the response of the system. In contrast, for an initial velocity of 0.34, the NO initially participates weakly in the response for the highest energies, but quickly begins to participate strongly after its dominant frequency aligns with and passes the tongue associated with the 3:1 IR of the underlying Hamiltonian system. This result verifies that the interactions and energy exchanges studied previously in this section are the result of a strongly nonlinear 3:1 IR between the LO and NO.

2.4 Loading scenario II: NO excited

In this subsection, we present the discussion and analysis of the energy flows between the LO and NO for loading scenario (LS) II. Recall that LS II corresponds to the case where the NO is excited using an initial velocity and all other initial conditions are zero. The response of the system was simulated for 2000 linearly spaced initial velocities in the range [0.001 1]. For each simulation, we estimate the total instantaneous energy in each mass using the procedure described in Sect. 2.1. The estimated energies are then normalized by the initial energy $\left(\frac{1}{2}v_0^2\right)$ and multiplied by 100% to obtain the instantaneous percent energy in each mass. We present the instantaneous percent energy as a function of initial velocity and time in Fig. 7a, b for the LO and NO, respectively. In contrast to LS I, where a large regime of energy isolation was observed, only a small regime of exists where the energy isolates in the NO. In fact, this regime only exists in the range of initial velocities of [0.001 0.1] compared to the range of [0.001 0.32] for the LS I. We refer to this regime as Regime I in the remainder of this subsection, and this is labeled in Fig. 7b. Outside of Regime I, the energy is shared between both the NO and the LO; however, this regime can be further divided into two separate regimes: first, we define Regime II as the portion corresponding to initial velocities of approximately 0.1 to 0.315; and, second, we define Regime III as the portion corresponding to

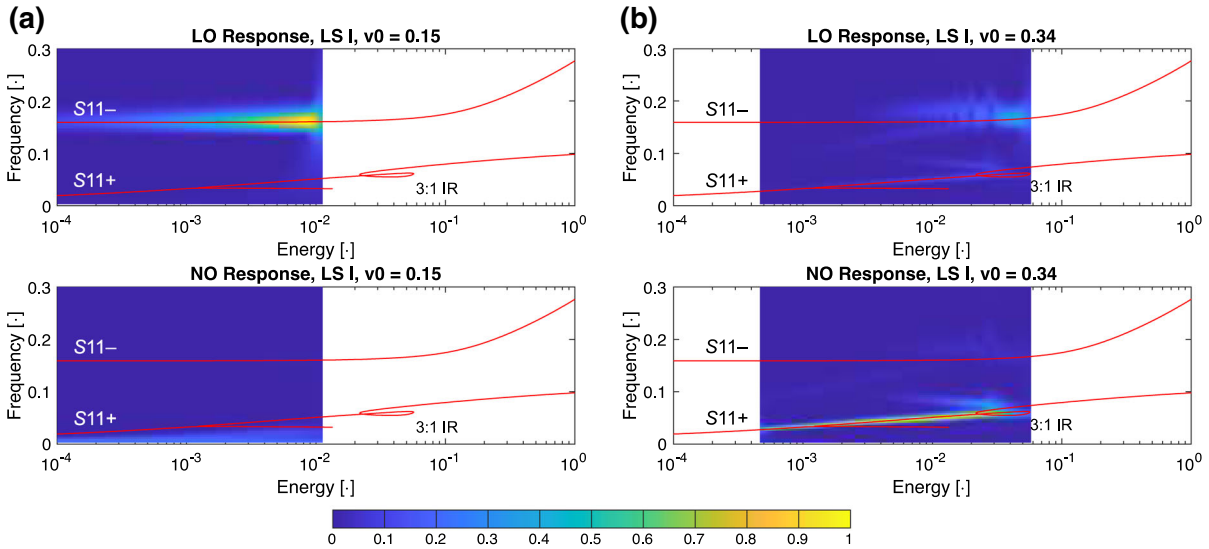

Fig. 6 Comparison of the NNMs of the underlying Hamiltonian system (shown in Fig. 2) with the wavelet spectra of the displacement response of the LO and NO for LS I and initial velocities of **a** 0.15 and **b** 0.34

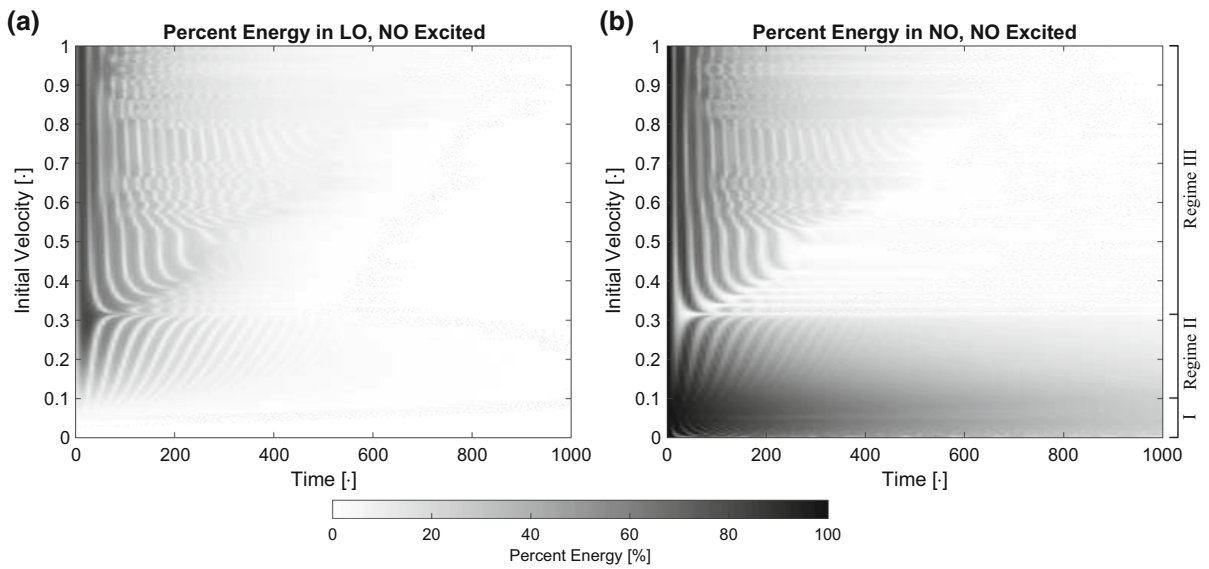

Fig. 7 The percent distribution of energy in the **a** LO and **b** NO as functions of time for LS II

initial velocities of approximately 0.315 to 1. These regimes are labeled in Fig. 7b. The major difference between Regimes II and III is the amount of energy shared between the LO and NO and which mass the energy concentrates in. In Regime II, the energy is primarily concentrated in the NO with only some of the energy being transferred to the LO. In contrast, in Regime III, significantly more energy is transferred to the LO and this results in faster dissipation than in Regime II. Furthermore, some initial velocities in Regime III result in an irreversible transfer of energy from the NO to the LO and these are represented by the appearance of the narrow white bands in Fig. 7b. For example, an initial velocity of 0.317 results in a complete and irreversible transfer of energy from the NO to the LO and we will study this case after further investigating Regime II.

To investigate Regime II, we consider the response of the system for an initial velocity of $v_0 = 0.15$ and plot the resulting displacement response in Fig. 8a. The comparison of the time series shows that the NO moves at a slower rate than the LO but achieves a significantly higher amplitude. In fact, the maximum displacement of the NO is 0.486, whereas that of the LO is 0.130, such that the NO displaces almost four times as much as the LO. Note that a similar trend can be observed for the velocities of the LO and NO, but we have excluded these here due to space considerations. To investigate the NNMs and harmonics that govern the response of each mass, we depict the corresponding WT spectra for each mass below the time series in Fig. 8a. The WT spectra reveal that the response of the LO is governed by multiple harmonics and NNMs. Specifically, the component with the lowest frequency corresponds to the first NNM of the system, which is primarily localized to the NO. The next two components are second sub- and third super-harmonics of the second and first NNMs, respectively. The next component is the second NNM with a frequency of approximately 1, and the last component is the fifth super-harmonic of the first NNM. Although the response of the NO is governed by the same components as the response of the LO, it is dominated by the first NNM and the other components only weakly participate in the response.

The WT reveal that, for this initial velocity, the frequencies of the first NNM and its harmonics are not high enough to interact with the second NNM, such that no IR arises in the dynamics. Consequently, only a some of the energy is transferred from the NO to the LO and a majority of the energy remains localized to the NO. To validate this conclusion, we present a comparison of the instantaneous total energy in each mass beneath the WT spectra in Fig. 8a. The comparison of the instantaneous total energies shows that a majority of the energy is localized to the NO and only a small amount is shared with the LO, which is indicated by the beating pattern in the two energies. Although the energy remains mostly concentrated in the NO, compared to LS I for the same initial velocity, a significant amount of energy is transferred to the LO. Recall that for LS I and an initial velocity of 0.15, the energy was almost completely isolated in the LO with the NO possessing at most 0.079% of the total energy at any time. In the present case, the LO possesses at

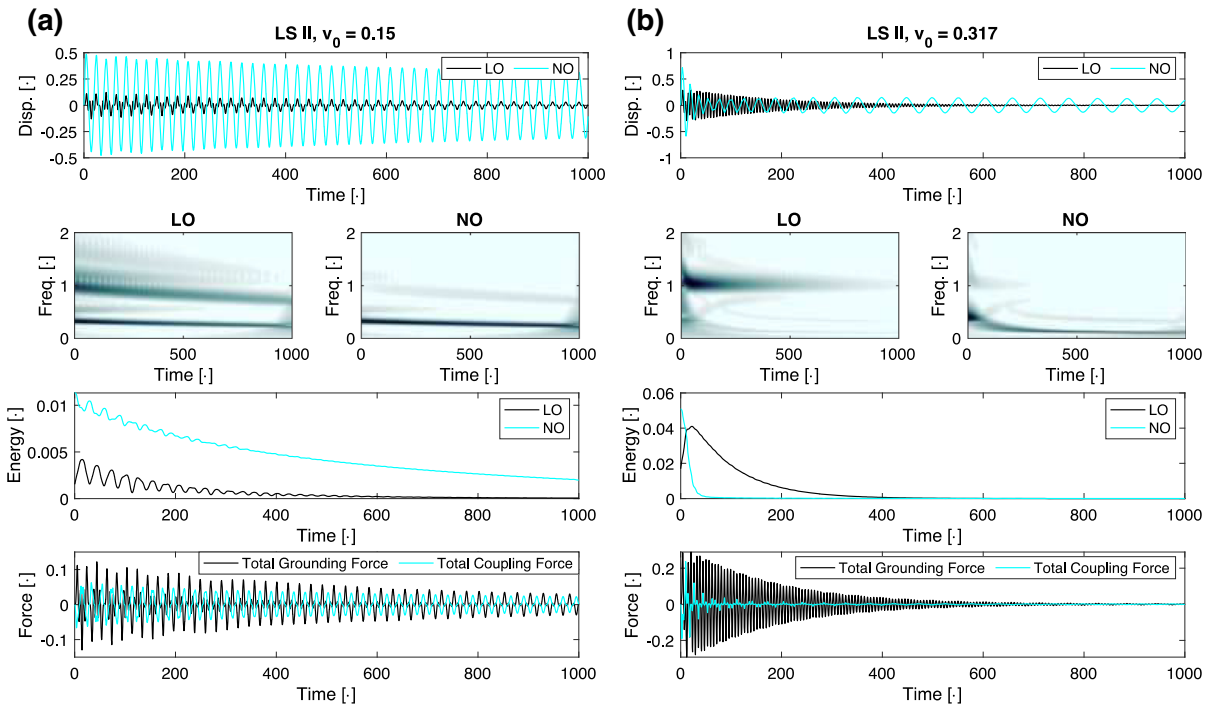

Fig. 8 Comparison of the displacement response, corresponding WT spectra and instantaneous energies for the LO and NO; and the grounding and coupling forces for LS II and initial velocities of **a** 0.15 and **b** 0.317

most 30.1% of the total energy in the system at any time. The fact that so much energy transfers to the LO when the NO is excited compared to the lack of energy transfer when the LO is excited indicates that there is a preferential direction of energy transfer (from the NO to the LO) in the dynamics. Looking now at the comparison of the total grounding and coupling forces, we find that the forces are comparable in magnitude even though the displacement of the NO is significantly larger than that of the LO. Recall that for LS I and this initial velocity, that the coupling forces was nearly zero, such that only active force was the grounding force which acts solely on the LO. The disparity between the forces in LS I and LS II further suggests that there is a preferential direction of energy transfer from the NO to the LO.

To further explore the suggested preferential direction of energy transfer, we turn to Regime III and consider the dynamics for an initial velocity of 0.317. This initial velocity corresponds to the center of the lowest white band in Fig. 7b, which represents a case where the energy is irreversibly transferred from the NO to the LO. Considering the displacement responses in Fig. 8b, we find that although the NO initially displaces more than twice as much as the LO, its amplitude diminishes so rapidly that after less than two cycles it displaces less than the LO. In fact, the NO has an initial displacement amplitude of 0.717 compared to 0.286 for the LO, but by a time of approximately 26, it has an amplitude of 0.269 compared to 0.280 for the LO. Furthermore, the amplitude of the LO actually decreases rather significantly in the beginning of the response before rapidly increasing, which indicates a beat arising from a nonlinear energy exchange between the NO and LO caused by an IR in the dynamics. Note that it takes approximately half as much time for the IR to arise in LS II than it does in LS I, where the IR only began after a time of 50, which further supports the claim that there is a preferential direction of energy transfer in the system.

To investigate the possibility of an IR in the response, we turn to a comparison of the WT spectra of the displacement responses of the LO and NO, which are presented below the displacement time series in Fig. 8b. Recall that the system is governed by two NNMs with the first and second NNMs primarily localized to the NO and LO, respectively. Additionally, because there is no linear coupling between the NO and the LO, the frequency of the first NNM depends strongly on the energy in the system (though mostly on the energy in the NO). The first and second NNMs are represented by the darkest bands in the WT spectrum of the displacement of the NO and LO, respectively. The WT spectra reveal that the initial frequencies of the first and second NNMs are approximately 0.383 and 1.15, respectively, such that the frequency of the second NNM is three times that of the first NNM. Thus, any energy exchanges in the response must result from a 3:1 IR between the first and second NNMs. Note that this is the same type of IR that was observed for in LS I for an initial velocity of 0.34, except that in LS I the second NNM was excited by exciting the LO and energy was transferred from a high frequency, the second NNM (LO), to a low frequency, the first NNM (NO). In the present case, the first NNM is excited directly by exciting the NO and energy is transferred from the first NNM (NO) at a low frequency to the second NNM (LO) at a high frequency.

Since the WT spectra are normalized to the same scale, where darker shading indicates higher energy content, we can directly compare the frequency content of the LO and NO. Initially, the energy is concentrated in the first NNM in the NO (darkest band in the WT spectrum of the NO), but this component rapidly decreases in not only energy (shading becomes lighter), but also frequency. Since the frequency of the first NNM is highly dependent on the energy in the NO, a decrease in frequency implies that the energy in the NO is also decreasing. Note that the rapid decrease in frequency of the first NNM is followed by a slow decreased in frequency starting around a time of 300 and a frequency of 0.125, which implies that the dissipation force acting on the NO is weak after this time. While the first NNM decreases in energy content and frequency, the second NNM actually increases in energy content and initially decreases in frequency before settling on its linear natural frequency of approximately 1. The observation that the second NNM in the WT spectrum of the displacement of the LO increases in energy content (shading gets darker) further suggests that energy is transferred into the LO from the NO.

To investigate the energy exchanges in the dynamics, we now turn to a comparison of the instantaneous total energies in the LO and NO presented below the WT spectra in Fig. 8b. The comparison of the energies

reveals that, although the NO begins with all of the energy, the energy is rapidly transferred to the LO where it remains trapped for the rest of the response. The irreversible nature of this energy transfer mimics that observed for a nonlinear energy sink installed on a LO, except that, in the present case, the LO actually behaves as a strongly nonlinear vibration absorber instead of the mass that has been "installed" on the LO. While subharmonic resonance in an LO–NES system results in irreversible transfer of energy from the LO to the NES [52], the 3:1 subharmonic IR results in the opposite behavior. Furthermore, the irreversibility of the energy transfer indicates that it is easier for the system to transfer energy from low to high frequencies than it is to transfer from high to low frequencies. Because it is easier for the system to transfer energy from low to high frequencies, a preferential direction of energy transfer from the NO to the LO arises in the dynamics because the first and second NNMs are localized to the NO and LO, respectively. We note that the comparison of the total grounding and coupling forces further reproduces and supports the observations made from the other parts of Fig. 8b.

Similar to Fig. 6, we verify that the 3:1 IR is responsible for the energy exchanges observed for this loading scenario. To this end, we superimpose the WT spectra of both the LO and NO on top of the NNMs for the underlying Hamiltonian system for initial velocities of 0.15 and 0.317 in Fig. 9a, b, respectively. For an initial velocity of 0.15, shown in Fig. 9a, the second NNM does not participate at all in the response and the majority of the motion is concentrated in the NO. Furthermore, we find that none of the IRs are activated for this velocity. In contrast, for an initial velocity of 0.317, all of the energy is initially concentrated in the NO, but as soon as the NO engages in the 3:1 IR a majority of the energy is irreversibly transferred to the LO. This result verifies that energy exchanges studied previously in this section are the result of a 3:1 IR between the LO and NO.

3 Experimental verification of targeted vibration isolation

3.1 System design and construction

To corroborate the previous computational results, we designed and constructed an experimental version of the LO–NO system out of aluminum and present the CAD model and resulting experimental system, Fig. 7a, b, respectively. The LO consists of a base platform, two sidewalls, two mounting rails, and two anchors. The LO base platform is constructed from an aluminum plate of dimensions 0.1524 m × 0.1524 m × 0.0127 m. The LO is grounded to an optical table using two L-shaped

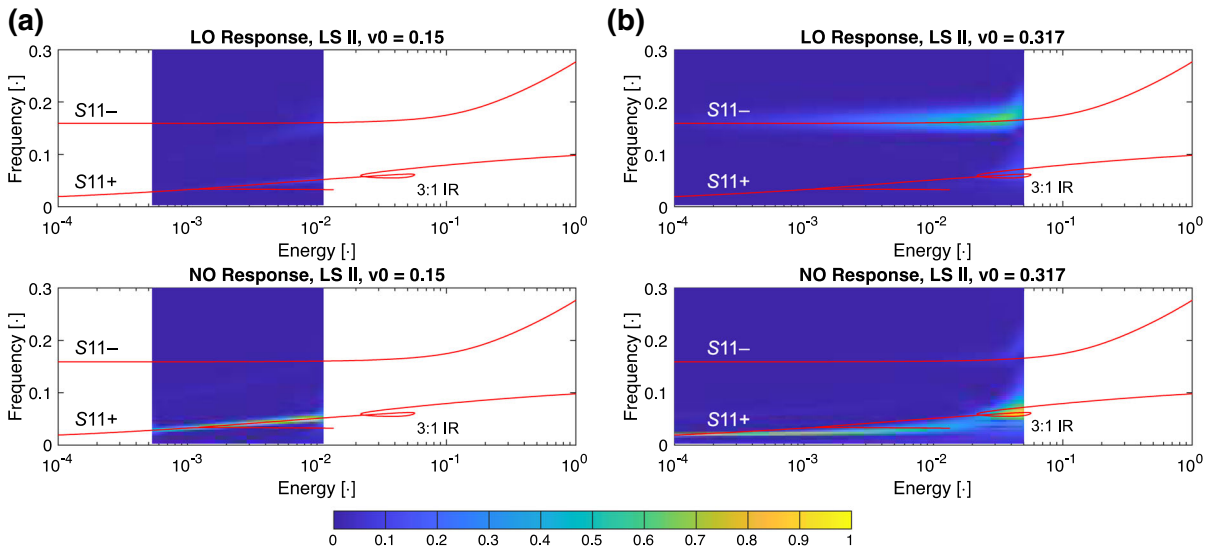

Fig. 9 Comparison of the NNMs of underlying Hamiltonian system (shown in Fig. 2) with the wavelet spectra of the displacement response of the LO and NO for LS II and initial velocities of **a** 0.15 and **b** 0.317

brackets, steel flexures, and 1/4″-20 UNC bolts. The steel flexures, which serve as linear grounding springs, are bolted to the L-shaped brackets and the LO base platform using 10–32 UNF bolts and have length, width, and thickness of 0.1143 m, 0.1524 m, and 0.00065 m, respectively. The LO is further composed of two aluminum rails (gray in Fig. 10a) and two aluminum sidewalls (purple in Fig. 7a) each equipped with an aluminum anchor (orange in Fig. 10a). The aluminum rails are used to mount thin steel flexures that linearly couple the NO to the LO and have dimensions 0.1524 m × 0.0127 m × 0.0127 m. The sidewalls are bolted to the LO base platform using two 10–32 UNF bolts and are constructed using aluminum plates with a length, width, and thickness of 0.1057 m, 0.127 m, and 0.00635 m, respectively. A large section of the sidewall was removed to minimize the mass as well as the friction between the sidewall and the LO base platform. An aluminum anchor is bolted onto each sidewall using two 10–32 UNF bolts, and these serve as clamping points for two thin steel wires that also clamp to the NO and introduce a strong, hardening stiffness nonlinearity into the dynamics of the system. The anchors are constructed out of aluminum blocks with dimensions 0.0254 m × 0.0126 m × 0.0508 m, and the wires are clamped to them using two 10–32 UNF set screws. The total mass of the assembled LO, including the flexures used to linearly couple the NO to the LO, is 1.370 kg.

The NO is composed of a base platform, one mounting rail, two sidewalls, and two anchors. The NO base platform is constructed from an aluminum plate of dimensions 0.1524 m × 0.1524 m × 0.0127 m. The NO is coupled to the LO using two thin steel flexures bolted on the sides using 10–32 UNF bolts and two thin steel wires clamped to the center of the NO using an aluminum mounting rail. The steel flexures provide a consistent linear stiffness coupling between the NO and the LO, whereas the wires introduce a strong stiffness nonlinearity due to geometric effects. The steel flexures have length and thickness of 0.1143 m and 0.003048 m, respectively. A large section was removed from the middle of the flexure to minimize the linear stiffness contribution, such that each flexure consists of two strips each with a width of 0.01905 m. The steel wires have a diameter of 0.000787 m, an active length of 0.127 m (i.e., the length between the anchors), and are clamped using 10–32 UNF set screws to an aluminum mounting rail installed on the bottom of the NO. The mounting rail is bolted to the NO using four 10–32 UNF bolts and has dimensions 0.1524 m × 0.0127 m × 0.0127 m. Originally, the assembled mass of the NO was 1.18 kg, so two extra aluminum plates and 31 extra washers were installed on the NO to increase its mass. The final assembled mass of the NO is 1.370 kg, such that the NO has as close to the same mass as the LO as could be measured.

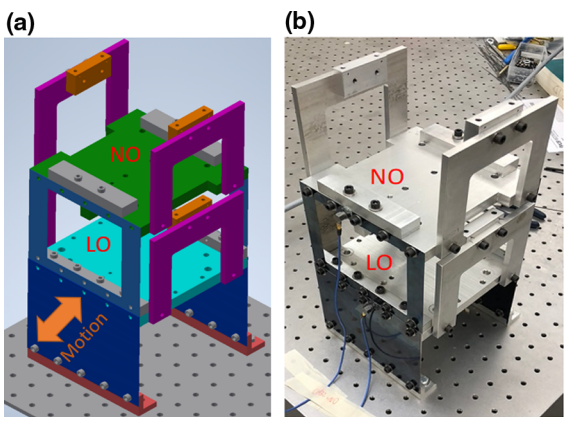

Fig. 10 **a** a CAD model representation of the LO–NO system and **b** the actual experimental implementation of the LO–NO system

3.2 Experimental measurements and nonlinear system identification

The experimental measurements consisted of two phases: first, we measured the response of the LO without the NO installed and used the resulting data to identify a linear model for the LO (described in the next paragraph). Second, we installed the NO and measured the free response of the coupled system, first, for loading scenario I (where the LO is excited) and, second, for loading scenario II (where the NO is excited). The excitation was realized by applying an impact using a PCB Piezotronics modal hammer (model 086C03) or PCB Piezotronics short-sledge hammer (model 086D20). The resulting free response was measured using PCB accelerometers (model 353B15) with nominal sensitivities of 1 mV/(m/s^2) using at a sampling rate of 16,384 Hz for 8 s using Abacus 906 hardware (Data Physics, San Jose, CA, USA) and the Data Physics Software Suite. The range was set to 10 V for all sensors to avoid cutting off large accelerations or impact forces. The accelerations were

numerically integrated and high-pass filtered using a third-order Butterworth filter with a cutoff frequency of 2 Hz to obtain the velocities of the LO and NO. This procedure was applied to the resulting velocities to produce the displacement response of the LO and NO.

As mentioned previously, the first experimental phase consisted of testing the LO without the NO installed and two measurements were performed for impacts of 35, 60.7, and 86 N. We present the displacement response and corresponding wavelet transform (WT) spectra for the 86 N measurement case in Fig. 11a and the corresponding frequency response function (FRF) in Fig. 11b. Without the NO installed, the LO is simply a harmonic oscillator governed by the equation

$$m_{\mathrm{LO}}\ddot{x} + d_1\dot{x} + k_1 x = F(t), \tag{3}$$

where $F(t)$ is the externally applied force. Since, in this configuration, the LO is linear and only has a single degree of freedom, the stiffness parameter, k_1,, can be calculated from the measured natural frequency of the oscillator, whereas the damping parameter, d_1,, can be identified directly from the FRF using procedures such as the half-power method. However, when we implemented the half-power method, it resulted in a damping ratio that was too large, and the simulated response decayed too quickly compared to the measurements. Thus, we employed the MFDID toolbox [57] to identify the damping ratio of the LO and calculated the stiffness directly from the measured natural frequency for the 86 N measurement case. The total mass of the LO, m_{LO}, was measured before the LO was bolted to the grounding flexures. This resulted in the following parameters: $m_{\mathrm{LO}} = 1.370$ kg, $d_1 = 2.177$ Ns/m ($\zeta = 0.00671$), and $k_1 = 19239$ N/m. To validate the identified model, we present a comparison of the simulated and measured responses of the LO for the measurement case used in the identification in Fig. 11a. Strong agreement is observed in both the time series and the corresponding WT spectra. Additionally, we also present a comparison of the FRFs of the measured and simulated responses in Fig. 11b, which shows that the identified model accurately reproduces the dynamics of the experimental LO.

After identifying the parameters for the LO, the NO was installed on the LO using both the steel flexures and the steel wires. In this configuration, the governing equations of motion are

$$\begin{aligned} &m_{\mathrm{LO}}\ddot{x} + d_1\dot{x} + d_2(\dot{x}-\dot{y}) + k_1 x + k_2(x-y) \\ &\quad +\alpha(x-y)|x-y|^{\beta} = 0, \end{aligned} \tag{4}$$

for LO and

$$m_{\mathrm{NO}}\ddot{y} + d_2(\dot{y}-\dot{x}) + k_2(y-x) + \alpha(y-x)|y-x|^{\beta} = F_2(t), \tag{5}$$

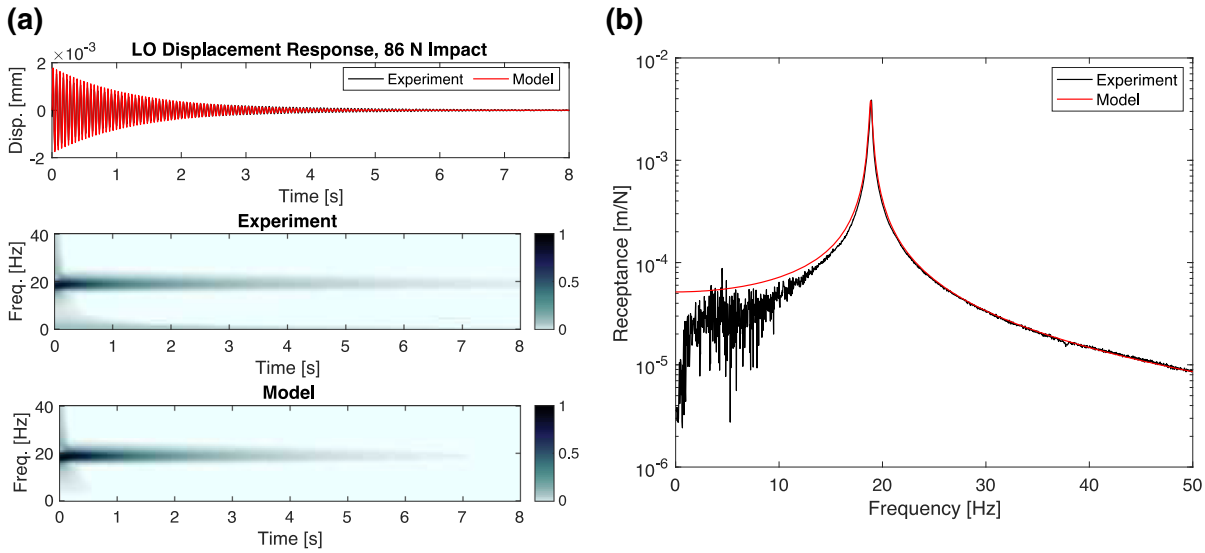

Fig. 11 **a** Displacement response and corresponding WT spectra of the LO without the NO installed measured experimentally and predicted using the identified model. **b** Comparison of the frequency–response functions computed using the measurement and the identified model

for the NO. Note that this is the same equations presented in 2.1, except that we have replaced the cubic nonlinearity with a generic polynomial nonlinearity. To identify the parameters governing the coupling between the LO and the NO, we attempted to isolate the dynamics of the NO by bolting the LO to the optical table using four 1/4″-20 UNC bolts; however, this introduced unwanted dynamics into the system and we were forced to identify the parameters using measurements where both the LO and NO were free to move. The measurement cases where the NO is excited are used to identify the coupling parameters because, under this loading scenario, the contribution of the nonlinearity is maximized compared to loading scenario where the LO is excited. Multiple measurements were taken for impacts ranging from 37 to 3500 N; however, only the case of an impact of 529 N was used for the identification and the displacement response, WT spectra, and FRFs for the LO and NO are presented in Fig. 12a, b, respectively.

To identify the unknown coupling parameters, we employed the method described in [25], which is a time-series-based optimization approach. Specifically, the response of the system is simulated numerically using the equations of motion in Eq. (4) and (5), and the coupling parameters are optimized to maximize the R-squared value between the simulated and measured responses for both the LO and NO. The optimization is performed using the *patternsearch* algorithm in MATLAB® with initial guesses of $k = 1900$ N/m, $\alpha = 2.5 \times 10^7$ N/m^3, $\beta = 2$, and $d = 1$ Ns/m. The upper and lower bounds are set such that $k_2 \in [0, 2500]$ N, $\alpha \in [10^7, 10^8]$ N/m$^{\beta+1}$, $\beta \in [1.5, 2.5]$, and $d_2 \in [0, 3]$ Ns/m. The identified parameters are $k = 1980.1$ N/m, $\alpha = 2.539 \times 10^7$ N/m$^{3.0002}$, $\beta = 2.0002$, and $d = 1.075$ Ns/m.

We present the identified parameters in Table 1 along with their corresponding nondimensional values as well as the nondimensional values used in the theoretical study. The nondimensionalization is set such that the mass of the LO, the linear grounding stiffness, and the nonlinear coupling stiffness are all equal to unity. We find that the nondimensional values of the identified parameters are comparable to the parameters used in the theoretical study, which confirms that the assembled LO–NO system is an experimental representation of the theoretical system. Moreover, we present the comparison of the simulated and measured responses for the LO and NO for the measurement case used in the identification in Fig. 12. We observe a good agreement between the simulated and measured responses in the time series as well as in the WT spectra and FRFs; however, a good agreement is expected because this measurement case was used to identify the coupling parameters. Thus, a stronger validation of the identified model comes from comparing simulated and measured responses for cases that were not used in the identification. To this end, we

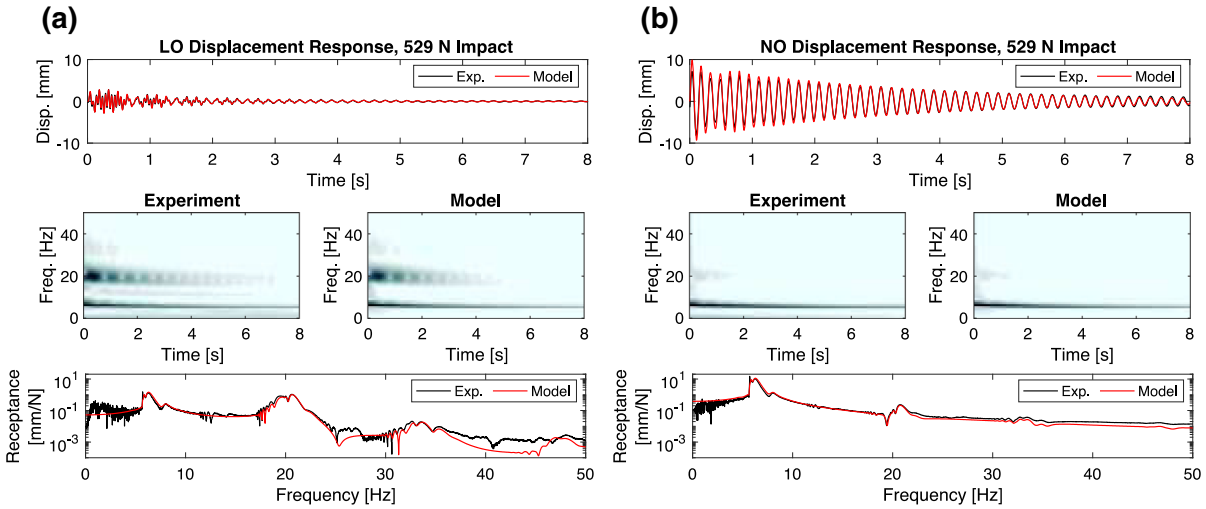

Fig. 12 Comparison of the measured and predicted responses for the measurement case used in the identification for **a** the LO and **b** the NO

Table 1 Parameters of LO–NO system

Parameter	Experimental dimensional	Experimental nondimensional	Theoretical nondimensional
m_{LO}	1.370 kg	1	1
m_{NO}	1.370 kg	1	1
k_1	19,239 N/m	1	1
d_1	2.177 Ns/m	0.0134	0.01
k_2	1980.1 N/m	0.1029	0
α	2.539×10^7 N/m$^{3.0002}$	1	1
β	2.0002	2.0002	2
d_2	1.075 Ns/m	0.0066	0.001

With nondimensional parameters used in computational study recorded in the second column, characterized parameters in the experiment in the third column and the corresponding nondimensional parameters on the fourth column

present a comparison between the simulated and measured responses of the LO and NO for impacts of 37 N and 898 N in Fig. 13a, b, respectively. Again, we observe good agreement between the simulated and measured responses, especially in early times when the nonlinearity is dominant, which validates the accuracy of the identified mathematical model for the experimental LO–NO system.

3.3 Experimental verification

To experimentally validate the behavior observed in the theoretical LO–NO system, we begin by constructing comparable energy flows using the same procedure described in Sect. 2.2. However, instead of applying an initial velocity, we apply the impulsive force

$$F(t) = P \sin\left(\frac{\pi}{0.0011} t\right)^2 (H(t) - H(t - 0.0011)), \tag{5}$$

where $P \in [1, 4000]$ N is representative of the forces achievable using a standard modal hammer with a soft red tip and $H(\cdot)$ is the Heaviside function. Note that the impulsive force has a duration of 0.0011 s and has zero amplitude at both $t = 0$ s and $t = 0.0011$ s. Just as in the theoretical study, we consider two forcing schemes: loading scenario (LS) I where the force is applied to the LO and no force is applied to the NO, and LS II where the force is applied to the NO and no force is applied to the LO. The range of forcing amplitudes corresponds to a range of nondimensional initial velocities of $v_0 \in [1.23 \times 10^{-4}, 0.492]$ for both LS I and II, such that all regimes are realizable for both LSs. The range of nondimensional velocities is computed using conservation of energy to obtain a dimensional velocity then nondimensionalizing that value. We consider 2000 linearly spaced values for P and compute the instantaneous percent energy in each mass using the same approach as in Sects. 2.3 and 2.4 and depict the resulting energy flows in Fig. 11a, b for LSs I and II, respectively.

As can be seen in Fig. 14a, in LS I, the energy localizes in the LO for $P < 1850$ N and no energy is transferred into the NO until $P \geq 1850$ N. Based on this observation, we partition the behavior of the LS I in the experimental system into the same Regimes I and II as in the theoretical system. Note that a force of 1850 N corresponds to a nondimensional velocity of 0.2275, which is lower than the nondimensional initial velocity of 0.32 that partitioned the behavior in the theoretical system. The decrease in the initial velocity needed to transition the behavior into Regime II results from the nonzero linear coupling stiffness, k_2, in the experimental system. Specifically, when the linear coupling stiffness is nonzero, the nonlinear mode corresponding to the motion of the NO possesses a nonzero natural frequency. As such, less energy is required in the system for the frequency of the NO to grow large enough for it to engage in a 3:1 IR with the LO.

To verify the existence of the two regimes in the experimental system under LS I, we compute the instantaneous total energy in each mass using the experimentally measured velocities and the procedure described in Sect. 2.2. We depict the resulting

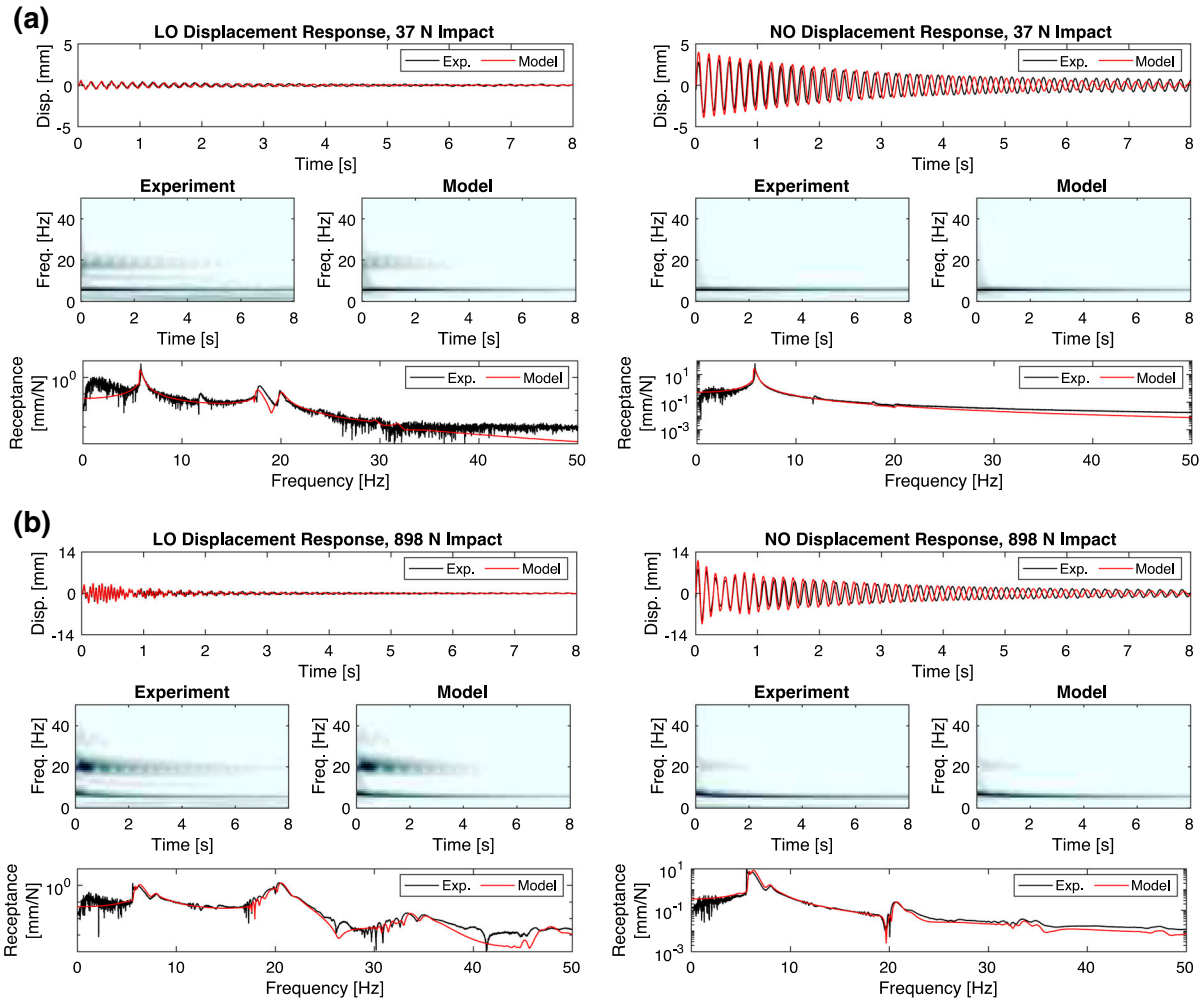

Fig. 13 Comparison of the measured and predicted responses of the LO and NO for impact forces of **a** 37 N and **b** 898 N, which were not used in the identification

energies for impulsive forces of 701, 1446, 2742, and 3879 N in Fig. 12a–d, respectively. Note that the energy flows shown in Fig. 14 are computed using the identified mathematical model for the experimental system, whereas Fig. 15 is constructed using the experimentally measured velocities and represents the observed behavior of the actual experimental system. The first two cases presented in Fig. 15 depict a localization of energy in LO with no energy being transferred to the NO through any mechanisms. These two cases confirm that no IR is activated in the dynamics inside Regime I of LS I in the experimental system, which validates that the extreme isolation of the NO from the LO predicted by the theoretical system can be realized physically. The last two cases presented in Fig. 15 both depict a beating pattern that indicates that the LO is exchanging energy with the NO and that the transfers of energy are reversible. The forces of these two cases correspond to first and second bands of energy transfer in LS I as shown in Fig. 14a and are the result of a the 3:1 IR between the LO and NO. Thus, the experimental results confirm the physical existence of both Regimes I and II as predicted by the theoretical system in Sect. 2.3.

Considering LS II now in Fig. 14b, we find that all three regimes observed in the theoretical study are captured by the energy distributions computed using the identified model for the experimental system. These regimes are labeled in Fig. 14b to aid in the discussion. Recall that, for LS II in the theoretical

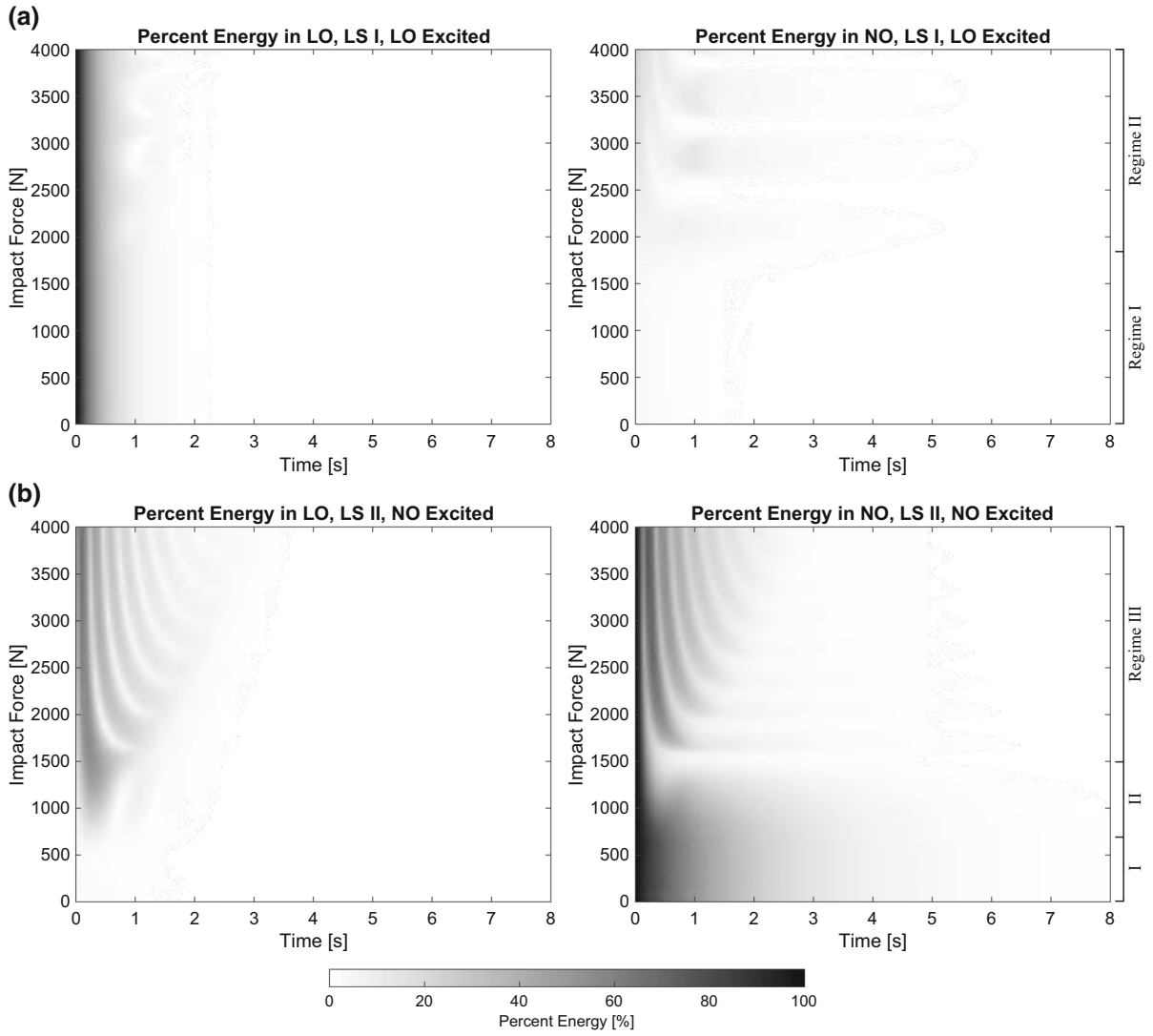

Fig. 14 The percent distribution of energy in the experimental LO and NO as functions of time for **a** LS I and **b** LS II

system, Regime I corresponded to complete localization of energy in the NO, Regime II corresponded to some sharing of energy between the two masses with the majority of the energy remaining in the NO, and Regime II corresponded to a significant exchange of energy with some cases resulting in complete and irreversible transfer of energy from the NO to the LO. The same three regimes are observed in Fig. 14b, and to verify the behavior in each of these regimes, we compute the instantaneous total energy in each mass using the procedure described in Sect. 2.2 and the experimentally measured velocities. We depict the resulting energies for impulsive forces of 37, 898, 1573, and 780 N (2760 N equivalent) in Fig. 13a–d, respectively. The first three cases were achieved using a PCB modal impact hammer (model 086C03), and the fourth case was realized using a PCB short-sledge hammer (model 086D20). Although the amplitude of the applied force in the fourth case is lower that of the second and third cases, the duration is substantially longer, such that the resulting work done on the NO is largest in the fourth case. Using impulse-momentum theory, we determined that the 780 N force has an equivalent amplitude of 2760 N if the smaller modal hammer was used to apply the same impulse to the NO. Note that the forcing cases of 37 N correspond to

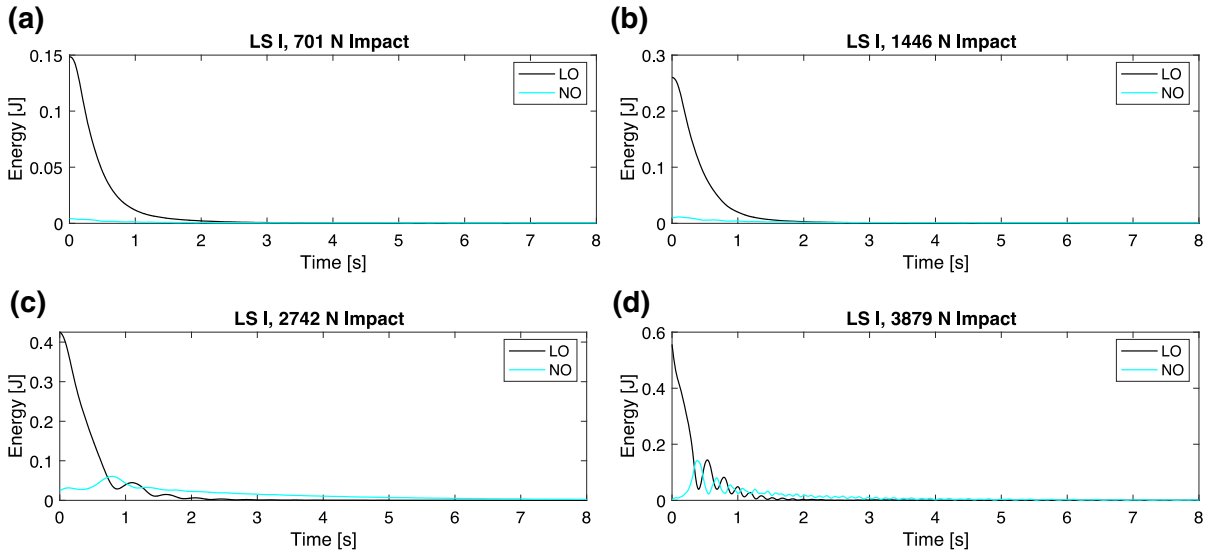

Fig. 15 The instantaneous total energies of the LO and NO for LS I (LO excited) for impulsive forcing of **a** 701 N, **b** 1446 N, **c** 2742 N, and **d** 3879 N. The modal hammer (PCB model 086D05) was used for all impulses shown

Regime I, 898 N to Regime II, and 1573 N and 780 N (2760 N equivalent) to Regime III. Two forcing cases are selected for Regime III to provide examples of complete irreversible energy transfer from the NO to the LO and significant exchanges of energy between the two masses leading into irreversible transfer.

Considering Fig. 16a, we find that the energy is localized to the NO for the duration of the measurement with only a small amount of energy present in the LO at any given time. The lack of energy exchanges between the NO and LO indicates that no IR is present in the response, such that the energy has no option but to localized in the NO. Thus, this experimental case

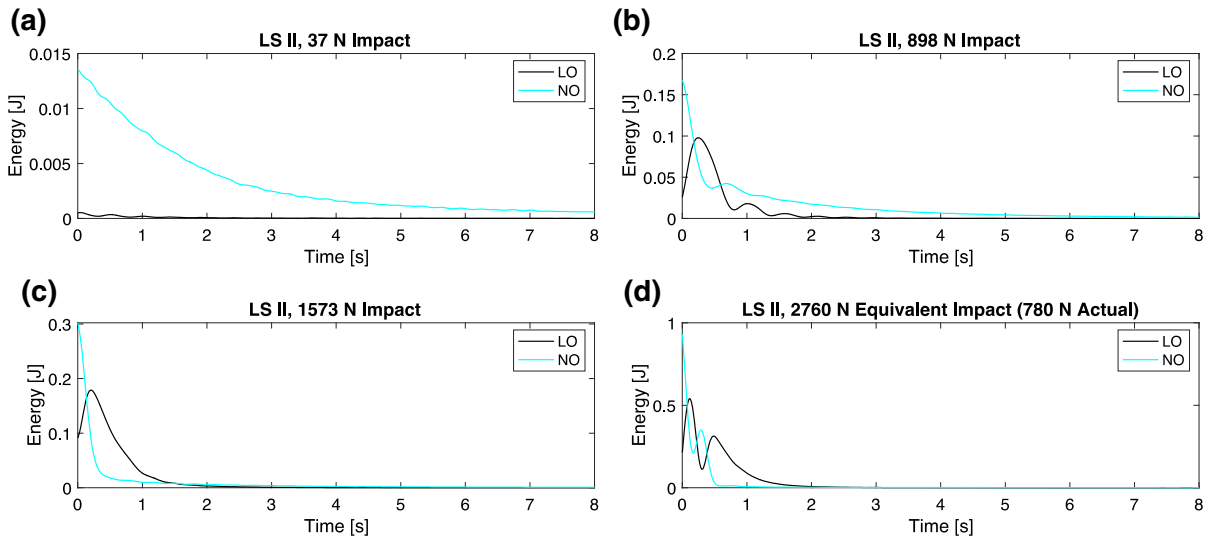

Fig. 16 The instantaneous total energies of the LO and NO for LS II (NO excited) for impulsive forcing of **a** 37 N, **b** 898 N, **c** 1573 N, and **d** 2760 N equivalent impact (780 N actual impact). Note that a modally tuned impulse hammer (PCB model 086D05) and a short-sledge impulse hammer (PCB model 086D20) were used to excite the system for (**a**–**c**) and (**d**), respectively

verifies the behavior observed in Regime I of the theoretical system and the identified model for the experimental system. Examining Fig. 16b, which depicts the energies for an impulsive force of 898 N, a clear beating pattern emerges in the energies that indicates that the NO and LO are exchanging energy. Although NO and LO are clearly exchanging energy, the instantaneous total energy of the NO is always greater than that of the LO, even when the energy the LO reaches a maximum during the beating cycle. Furthermore, the majority of the energy remains in the NO for the entire measurement. These two observations indicate that no IR is present in the responses, which verifies the predictions of both the theoretical system and the identified model for Regime II in LS II.

Looking now at Fig. 16c, which depicts the energies for a forcing of 1573 N and is the first case in Regime III, we find that the energy is rapidly and irreversibly transferred to the Lo where it is quickly dissipated. The fact that the energy is transferred to the LO and never returns to the NO indicates that a strong IR is present in the dynamics, which is the same 3:1 IR between the first and second NNMs that was observed in the investigation of the theoretical system. Furthermore, the energy transfer observed verifies that a preferential direction of energy transfer from the NO to the LO exists in the dynamics. The preferential direction of energy transfer arises because it is easier for energy to be transferred from low to high frequencies (first to second NNM) than it is for energy to transfer from high to low frequencies. These results experimentally validate the predictions of the theoretical system and the identified model and verify the prediction of a preferential direction of energy transfer. Finally, considering Fig. 16d, which depicts the energies for a forcing of 780 N (2760 N equivalent) and is also in Regime III, we find that initially a strong beating pattern appears where the energy oscillates between the NO and LO. However, this exchange of energy is extremely short-lived, ceasing at a time of 0.29 s, where the energy is irreversibly transferred to the LO. Moreover, the large transfers of energy from the NO to the LO cause the motion to rapidly decay compared to the observed dissipation trends in Regimes I and II. Based on these results, we conclude that all three regimes observed in the theoretical system for LS II are experimentally realizable and that the observed energy flows are indeed physical.

4 Concluding remarks

This research focused on the flow of mechanical energy between two nonlinearly coupled oscillators with comparable mass. The first oscillator was connected to ground using a linear spring and damper, and it represents the prototypical linear oscillator (LO) that is often used in studies of energy transfer. The second oscillator was coupled to the LO using a weak linear spring, weak linear damper, and a strong nonlinear spring with a polynomial restoring force relationship, and we called this oscillator the nonlinear oscillator (NO) in the system. The resulting system possessed two nonlinear normal modes (NNMs) with the first and second NNMs localized to the NO and LO, respectively. The dynamics of the system was investigated both theoretically using a nondimensional model and experimentally using a physical model. In both cases, we studied the dynamics for two loading scenarios (LSs): in LS I, the LO was excited using an initial velocity for the theoretical system and an impulsive force in the experimental system, while the NO began at rest; and in LS II, the NO was excited using either an initial velocity or an impulsive force, while the LO began at rest.

In the theoretical system for LS I, we observed that the energy flows could be portioned into two separate regimes. In the first regime, the energy was found to localize in the LO and no energy was shared with the NO. In the second regime, the energy was found to initially localize in the LO, but was then shared and exchanged with the NO. The energy exchanges were the result of a 3:1 internal resonance (IR) between the first and second NNMs where energy was transferred from the second NNM at high frequency to the first NNM at low frequency. Using the experimental system, we verified the behavior in Regime I, but we were unable to reproduce the behavior observed in Regime II due to limitations in the force that could be realized without damaging the structure. For LS II, we observed that the energy flows could be partitioned into three different regimes. In the first regime, the energy was localized to the NO for the entire duration of the response and no energy was transferred to the LO. In Regime II, some of the energy was exchanged between the NO and LO, but the majority remained localized in the NO for the duration of the response. In Regime III, strong energy exchanges between the NO and LO were observed and, in some cases, all of the

energy was irreversibly transferred to the LO. Based on an analysis of the NNMs, we concluded that the energy transfer in Regime III resulted from a 3:1 IR between the first and second NNMs—the same IR as that observed in Regime II for LS I, except that, in this case, the energy transferred from the first NNM at low frequency to the second NNM at high frequency. We found that substantially more energy was transferred by the IR in LS II than in LS I in the present case than in the IR observed in LS I, which led to the conclusion that it is easier for the system to transfer energy from low to high frequencies. Moreover, because the first and second NNMs are localized to the NO and LO, respectively, we concluded that the system possessed a preferential direction of energy transfer: from the NO to the LO. All three regimes for LS II and the accompanying observations were reproduced and verified using the experimental system including the case of irreversible energy transfer and the preferential direction of energy transfer.

Typical studies of energy transfer in mechanical oscillators focus on the phenomena of targeted energy transfer and the use of a nonlinear energy sink (NES) dissipates vibrations. In such studies, the NES is assumed to be an attachment that is installed on a linear primary structure. The NES then acts like a parasite by irreversibly stealing energy from the primary structure and rapidly dissipating it. In the current research, the NO should not be thought of as an attachment installed on a linear primary structure (i.e., the LO). Rather, one of two viewpoints should be taken. First, the NO can be thought of as a vibration-sensitive piece of equipment that we wish to isolate from its surroundings, so long as the vibration levels remain in Regime I of LS I. In this case, the LO acts as a vibration isolation system that is installed between the NO and ground with the intent to isolate the NO. Future research is dedicated to determining the effectiveness of this type of system for vibration isolation under base excitation and forced harmonic excitation. Second, we can consider both the LO and NO to be integral components of the overall system and, in this case, our objective is to passively manipulate and control the flow of energy between the two components. Another possible application is to building design and the mitigation of seismic motion by isolating the incoming energy to the bottom of the building. In this context, the LO represents the second floor of the building and the NO represents either the third floor or all other floors lumped together as one. The second floor then acts as an energy sink that localizes the energy introduced by the seismic motion in itself and prevents that energy from propagating upward into the rest of the building. Moreover, this approach opens the way for incorporating vibration mitigation directly into the primary structure without the need for additional vibration absorbers such as NESs. Although NESs hold a near monopoly on the discussion and research on targeted energy transfer in mechanical oscillators, the research presented here demonstrates that there is still much to learn about energy transfer in general and that many more applications beyond the standard definition of targeted energy transfer are possible.

Funding No funding was provided for this study.

Compliance with ethical standards

Conflict of interest The authors declare that there are no conflicts of interest or competing interests regarding the publication of this article.

References

1. Vakakis, A.F., Gendelman, O.V., Bergman, L.A., McFarland, D.M., Kerschen, G., Lee, Y.S.: Nonlinear targeted energy transfer in mechanical and structural systems I. (2008)
2. Vakakis, A.F.: Passive nonlinear targeted energy transfer. Philos. Trans. R. Soc. Lond. A Math., Phys. Eng. Sci. **376**, 20170132 (2018). https://doi.org/10.1098/rsta.2017.0132
3. Lee, Y.S., Vakakis, A.F., Bergman, L.A., McFarland, D.M., Kerschen, G.: Enhancing the robustness of aeroelastic instability suppression using multi-degree-of-freedom nonlinear energy sinks. AIAA J. **46**, 1371–1394 (2008). https://doi.org/10.2514/1.30302
4. AL-Shudeifat, M.A., Wierschem, N., Vakakis, A.F., Bergman, L.A., Spencer, Jr., Billie F.: Numerical and experimental investigation of a new nonlinear energy sink for passive shock mitigation. 1161–1164 (2012). https://doi.org/https://doi.org/10.1115/DETC2012-70453
5. Hubbard, S.A., McFarland, D.M., Bergman, L.A., Vakakis, A.F.: Targeted energy transfer between a model flexible wing and nonlinear energy sink. J. Aircraft. **47**, 1918–1931 (2010). https://doi.org/10.2514/1.C001012
6. Hubbard, S.A., McFarland, D.M., Bergman, L.A., Vakakis, A.F., Andersen, G.: Targeted energy transfer between a swept wing and winglet-housed nonlinear energy sink. AIAA J. **52**, 2633–2651 (2014). https://doi.org/10.2514/1.J052538
7. Luongo, A., Zulli, D.: Nonlinear energy sink to control elastic strings: the internal resonance case. Nonlinear Dyn. **81**, 425–435 (2015)

8. Gourc, E., Seguy, S., Michon, G., Berlioz, A., Mann, B.P.: Quenching chatter instability in turning process with a vibro-impact nonlinear energy sink. J. Sound Vib. **355**, 392–406 (2015)
9. Bichiou, Y., Hajj, M.R., Nayfeh, A.H.: Effectiveness of a nonlinear energy sink in the control of an aeroelastic system. Nonlinear Dyn. **86**, 2161–2177 (2016)
10. Darabi, A., Leamy, M.J.: Clearance-type nonlinear energy sinks for enhancing performance in electroacoustic wave energy harvesting. Nonlinear Dyn. **87**, 2127–2146 (2017)
11. Yang, K., Zhang, Y.-W., Ding, H., Yang, T.-Z., Li, Y., Chen, L.-Q.: Nonlinear energy sink for whole-spacecraft vibration reduction. J. Vib. Acoust. **139**, 021011–19 (2017)
12. Zhang, Y.-W., Yuan, B., Fang, B., Chen, L.-Q.: Reducing thermal shock-induced vibration of an axially moving beam via a nonlinear energy sink. Nonlinear Dyn. **87**, 1159–1167 (2017)
13. Ebrahimzade, N., Dardel, M., Shafaghat, R.: Investigating the aeroelastic behaviors of rotor blades with nonlinear energy sinks. AIAA J. **56**, 2856–2869 (2018). https://doi.org/10.2514/1.J056530
14. Gendelman, O., Manevitch, L.I., Vakakis, A.F., M'Closkey, R.: Energy pumping in nonlinear mechanical oscillators: Part I–dynamics of the underlying Hamiltonian systems. J. Appl. Mech., Trans. ASME. **68**, 34–41 (2001)
15. Vakakis, A.F., Gendelman, O.: Energy pumping in nonlinear mechanical oscillators: Part II–resonance capture. J. Appl. Mech. Trans. ASME. **68**, 42–48 (2001). https://doi.org/10.1115/1.1345525
16. McFarland, D.M., Bergman, L.A., Vakakis, A.F.: Experimental study of non-linear energy pumping occurring at a single fast frequency. Int. J. Nonlinear Mech. **40**, 891–899 (2005). https://doi.org/10.1016/j.ijnonlinmec.2004.11.001
17. Moore, K.J., Kurt, M., Eriten, M., McFarland, D.M., Bergman, L.A., Vakakis, A.F.: Time-series-based nonlinear system identification of strongly nonlinear attachments. J. Sound Vib. **438**, 13–32 (2019). https://doi.org/10.1016/j.jsv.2018.09.033
18. Qiu, D., Li, T., Seguy, S., Paredes, M.: Efficient targeted energy transfer of bistable nonlinear energy sink: application to optimal design. Nonlinear Dyn. **92**, 443–461 (2018). https://doi.org/10.1007/s11071-018-4067-7
19. AL-Shudeifat, M.A., Saeed, A.S.: Frequency-energy dependence of the bistable nonlinear energy sink. In: ASME International Design Engineering Technical Conferences and Computers and Information in Engineering Conference, Volume 8: 29th Conference on Mechanical Vibration and Noise, p. V008T12A022. ASME, Cleveland, OH (2017)
20. Habib, G., Romeo, F.: The tuned bistable nonlinear energy sink. Nonlinear Dyn. **89**, 179–196 (2017). https://doi.org/10.1007/s11071-017-3444-y
21. Lee, Y.S., Nucera, F., Vakakis, A.F., McFarland, D.M., Bergman, L.A.: Periodic orbits, damped transitions and targeted energy transfers in oscillators with vibro-impact attachments. Physica D **238**, 1868–1896 (2009). https://doi.org/10.1016/j.physd.2009.06.013
22. Wang, J., Wierschem, N., Spencer, B.F., Lu, X.: Numerical and experimental study of the performance of a single-sided vibro-impact track nonlinear energy sink. Earthq. Eng. Struct. Dyn. **45**, 635–652 (2016). https://doi.org/10.1002/eqe.2677
23. Li, T., Gourc, E., Seguy, S., Berlioz, A.: Dynamics of two vibro-impact nonlinear energy sinks in parallel under periodic and transient excitations. Int. J. Non-Linear Mech. **90**, 100–110 (2017)
24. Li, T., Seguy, S., Berlioz, A.: On the dynamics around targeted energy transfer for vibro-impact nonlinear energy sink. Nonlinear Dyn. **87**, 1453–1466 (2017)
25. Moore, K.J., Bunyan, J., Tawfick, S., Gendelman, O.V., Shuangbao, L., Leamy, M.J., Vakakis, A.F.: Non-reciprocity in the dynamics of coupled oscillators with nonlinearity, asymmetry and scale hierarchy. Phys. Rev. E. **97**, 012219 (2018)
26. Bunyan, J., Moore, K.J., Mojahed, A., Fronk, M.D., Leamy, M., Tawfick, S., Vakakis, A.F.: Acoustic nonreciprocity in a lattice incorporating nonlinearity, asymmetry, and internal scale hierarchy: experimental study. Phys. Rev. E. **97**, 052211 (2018). https://doi.org/10.1103/PhysRevE.97.052211
27. Fronk, M.D., Tawfick, S., Daraio, C., Li, S., Vakakis, A., Leamy, M.J.: Acoustic non-reciprocity in lattices with nonlinearity, internal hierarchy, and asymmetry: computational study. J. Vib. Acoust. (2019). https://doi.org/10.1115/1.4043783
28. Blanchard, A., Sapsis, T.P., Vakakis, A.F.: Non-reciprocity in nonlinear elastodynamics. J. Sound Vib. **412**, 326–335 (2018). https://doi.org/10.1016/j.jsv.2017.09.039
29. Moore, K.J., Vakakis, A.F.: Wave non-reciprocity at a nonlinear structural interface. Acta Mech. **229**, 4057–4070 (2018). https://doi.org/10.1007/s00707-018-2212-5
30. Chen, Y., Li, X., Nassar, H., Norris, A.N., Daraio, C., Huang, G.: Nonreciprocal wave propagation in a continuum-based metamaterial with space-time modulated resonators. Phys. Rev. Appl. **11**, 064052 (2019). https://doi.org/10.1103/PhysRevApplied.11.064052
31. Mojahed, A., Bunyan, J., Tawfick, S., Vakakis, A.F.: Tunable acoustic nonreciprocity in strongly nonlinear waveguides with asymmetry. Phys. Rev. Appl. **12**, 034033 (2019). https://doi.org/10.1103/PhysRevApplied.12.034033
32. Fang, L., Darabi, A., Mojahed, A., Vakakis, A.F., Leamy, M.J.: Broadband non-reciprocity with robust signal integrity in a triangle-shaped nonlinear 1D metamaterial. Nonlinear Dyn. **100**, 1–13 (2020). https://doi.org/10.1007/s11071-020-05520-x
33. Dantas, M.J.H., Balthazar, J.M.: On energy transfer between linear and nonlinear oscillators. J. Sound Vib. **315**, 1047–1070 (2008). https://doi.org/10.1016/j.jsv.2008.02.033
34. Costa, S.N.J., Hassmann, C.H.G., Balthazar, J.M., Dantas, M.J.H.: On energy transfer between vibrating systems under linear and nonlinear interactions. Nonlinear Dyn. **57**, 57–67 (2009). https://doi.org/10.1007/s11071-008-9419-2
35. Pilipchuk, V.N.: Analytical study of vibrating systems with strong non-linearities by employing saw-tooth time transformations. J. Sound Vib. **192**, 43–64 (1996)
36. Manevitch, L.I.: The description of localized normal modes in a chain of nonlinear coupled oscillators using complex variables. Nonlinear Dyn. **25**, 95–109 (2001). https://doi.org/10.1023/A:1012994430793
37. Kerschen, G., Vakakis, A.F., Lee, Y.S., Mcfarland, D.M., Kowtko, J.J., Bergman, L.A.: Energy transfers in a system of two coupled oscillators with essential nonlinearity: 1:1

resonance manifold and transient bridging orbits. Nonlinear Dyn. **42**, 283–303 (2005). https://doi.org/10.1007/s11071-005-4475-3
38. Lamarque, C.-H., Gendelman, O.V., Ture Savadkoohi, A., Etcheverria, E.: Targeted energy transfer in mechanical systems by means of non-smooth nonlinear energy sink. Acta Mech. **221**, 175 (2011). https://doi.org/10.1007/s00707-011-0492-0
39. Kurt, M., Eriten, M., McFarland, D.M., Bergman, L.A., Vakakis, A.F.: Strongly nonlinear beats in the dynamics of an elastic system with a strong local stiffness nonlinearity: analysis and identification. J. Sound Vib. **333**, 2054–2072 (2014). https://doi.org/10.1016/j.jsv.2013.11.021
40. Kurt, M., Eriten, M., McFarland, D.M., Bergman, L.A., Vakakis, A.F.: Frequency–energy plots of steady-state solutions for forced and damped systems, and vibration isolation by nonlinear mode localization. Commun. Nonlinear Sci. Numer. Simul. **19**, 2905–2917 (2014). https://doi.org/10.1016/j.cnsns.2013.12.018
41. Kurt, M., Slavkin, I., Eriten, M., McFarland, D.M., Gendelman, O.V., Bergman, L.A., Vakakis, A.F.: Effect of 1:3 resonance on the steady-state dynamics of a forced strongly nonlinear oscillator with a linear light attachment. Arch Appl Mech. **84**, 1189–1203 (2014). https://doi.org/10.1007/s00419-014-0877-3
42. Manevitch, L.I., Koroleva, I.P.: Limiting phase trajectories as an alternative to nonlinear normal modes. Procedia IUTAM. **19**, 144–151 (2016). https://doi.org/10.1016/j.piutam.2016.03.019
43. Yacobi, G., Kislovsky, V., Kovaleva, M., Starosvetsky, Y.: Unidirectional energy transport in the symmetric system of non-linearly coupled oscillators and oscillatory chains. Nonlinear Dyn. **98**, 2687–2709 (2019). https://doi.org/10.1007/s11071-019-05230-z
44. Nayfeh, A.H., Mook, D.T.: Nonlinear Oscillations. Wiley, New York (1995)
45. Silva, P.B., Leamy, M.J., Geers, M.G.D., Kouznetsova, V.G.: Application of the method of multiple scales to unravel energy exchange in nonlinear locally resonant metamaterials. https://arxiv.org/abs/1812.05713 [cond-mat, physics:physics]. (2018)
46. Silva, P.B., Leamy, M.J., Geers, M.G.D., Kouznetsova, V.G.: Emergent subharmonic band gaps in nonlinear locally resonant metamaterials induced by autoparametric resonance. Phys. Rev. E. **99**, 063003 (2019). https://doi.org/10.1103/PhysRevE.99.063003
47. Luongo, A., Zulli, D.: Dynamic analysis of externally excited NES-controlled systems via a mixed multiple scale/harmonic balance algorithm. Nonlinear Dyn. **70**, 2049–2061 (2012). https://doi.org/10.1007/s11071-012-0597-6
48. Sapsis, T., Quinn, D.D., Vakakis, A.F., Bergman, L.A.: Effective stiffening and damping enhancement of structures with strongly nonlinear local attachments. J. Vib. Acoust. **134**, 011016–01101612 (2012). https://doi.org/10.1115/1.4005005
49. Kerschen, G., Kowtko, J.J., Mcfarland, D.M., Bergman, L.A., Vakakis, A.F.: Theoretical and experimental study of multimodal targeted energy transfer in a system of coupled oscillators. Nonlinear Dyn. **47**, 285–309 (2007). https://doi.org/10.1007/s11071-006-9073-5
50. Oliva, M., Barone, G., Navarra, G.: Optimal design of Nonlinear Energy Sinks for SDOF structures subjected to white noise base excitations. Eng. Struct. **145**, 135–152 (2017)
51. Chen, Y.: A Non-Model Based Expansion Methodology for Dynamic Characterization. PhD diss., University of Massachusetts Lowell (2019)
52. Silva, C.E., Maghareh, A., Tao, H., Dyke, S.J., Gibert, J.: Evaluation of energy and power flow in a nonlinear energy sink attached to a linear primary oscillator. J. Vib. Acoust. (2019). https://doi.org/10.1115/1.4044450
53. Vakakis, A.F., Manevitch, L.I., Mikhlin, Y.V., Pilipchuk, V.N., Zevin, A.: Normal Modes and Localization of Nonlinear Systems. Wiley, New York (1996)
54. Kerschen, G., Peeters, M., Golinval, J.C., Vakakis, A.F.: Nonlinear normal modes, Part I: a useful framework for the structural dynamicist. Mech. Syst. Signal Process. **23**, 170–194 (2009). https://doi.org/10.1016/j.ymssp.2008.04.002
55. Peeters, M., Viguié, R., Sérandour, G., Kerschen, G., Golinval, J.-C.: Nonlinear normal modes, Part II: toward a practical computation using numerical continuation techniques. Mech. Syst. Signal Process. **23**, 195–216 (2009). https://doi.org/10.1016/j.ymssp.2008.04.003
56. Addison, P.S.: The illustrated wavelet transform handbook introductory theory and applications in science, engineering, medicine and finance. Taylor & Francis, New York (2002)
57. Kim Saang, B., Spencer, B.F., Yun, C.-B.: Frequency domain identification of multi-input, multi-output systems considering physical relationships between measured variables. J Eng. Mech. **131**, 461–472 (2005). https://doi.org/10.1061/(ASCE)0733-9399(2005)131:5(461)